AD-A040 051 HARVARD UNIV CAMBRIDGE MASS GORDON MCKAY LAB F/G 20/14
THE BEVERAGE WAVE ANTENNA: RADIATION FIELD PATTERNS,(U)
FEB 77 R M SORBELLO F19628-76-C-0057
UNCLASSIFIED SCIENTIFIC-2 RADC-TR-77-83 NL

| OF |
AD
A040051

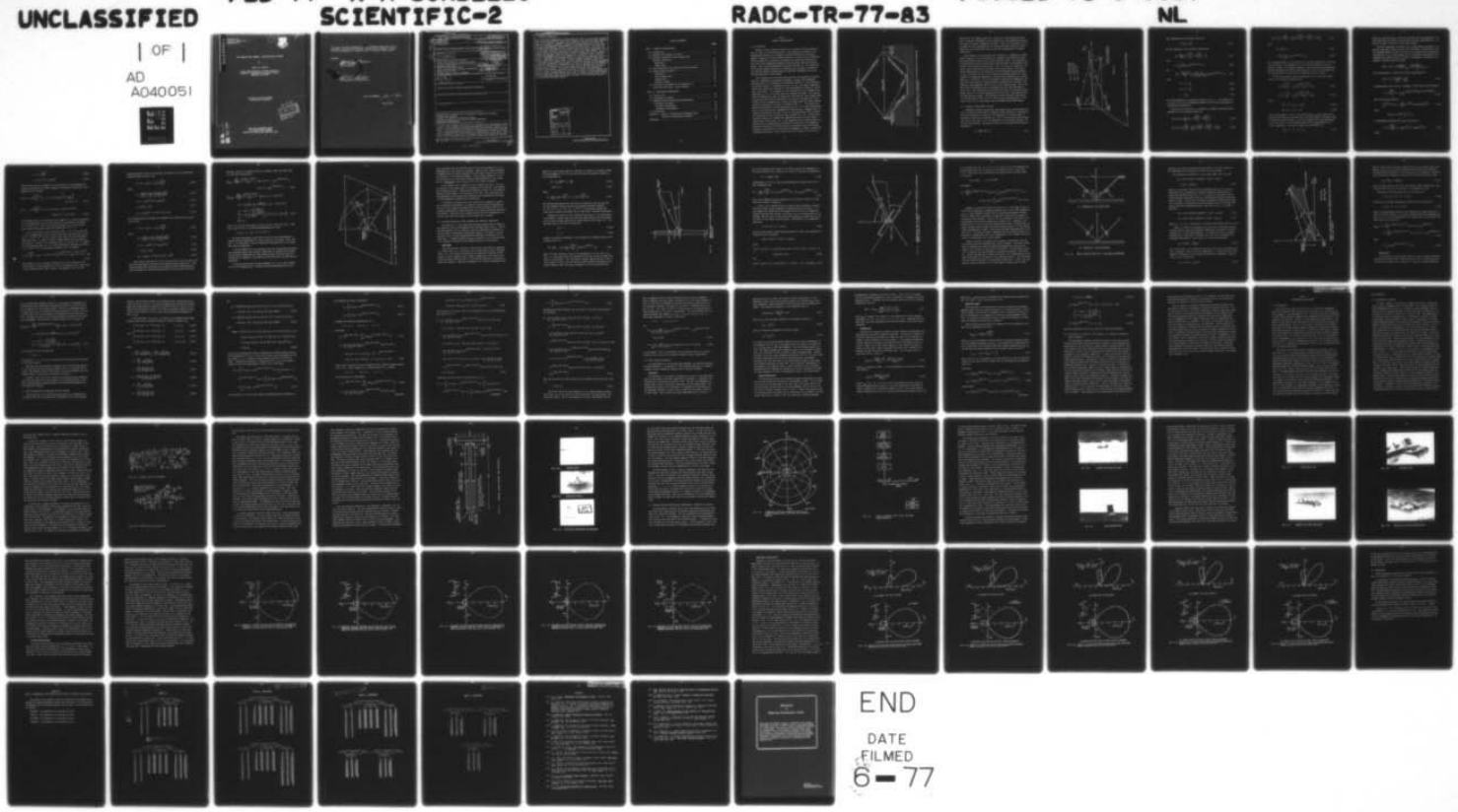

END

DATE
FILMED
6-77

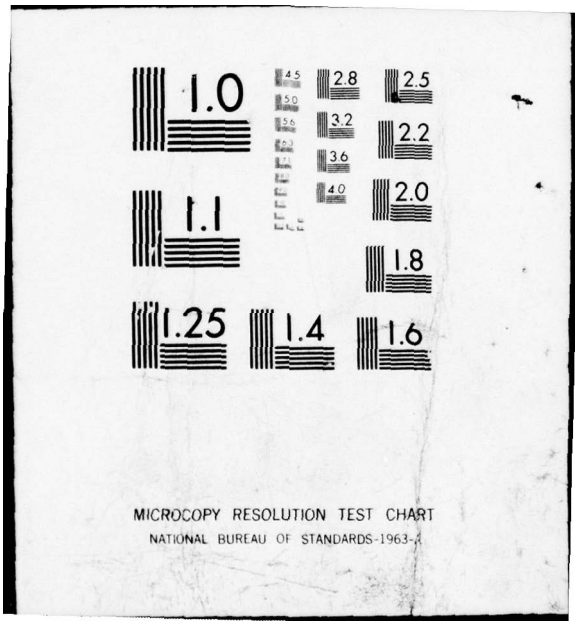
1.0
1.1
1.25
1.4
1.6
1.8
2.0
2.2
2.5
2.8
3.2
3.6
4.0
4.5
5.0
5.6
MICROCOPY RESOLUTION TEST CHART
NATIONAL BUREAU OF STANDARDS-1963-A

RADC-TR-77-83
Scientific Report No. 2
February 1977

(12)

THE BEVERAGE WAVE ANTENNA: RADIATION FIELD PATTERNS

by

Robert M. Sorbello

Gordon McKay Laboratory, Harvard University
Division of Engineering and Applied Physics
Cambridge, MA 02138

Approved for public release;
distribution unlimited.

ROME AIR DEVELOPMENT CENTER
AIR FORCE SYSTEMS COMMAND
GRIFFISS AIR FORCE BASE, NEW YORK 13441

This report has been reviewed by the RADC Information Office (OI) and is releasable to the National Technical Information Service (NTIS). At NTIS it will be releasable to the general public, including foreign nations.

APPROVED:

JOHN F. McILVENNA
Project Engineer

APPROVED:

ALLAN C. SCHELL, Acting Chief
Electromagnetic Sciences Division

FOR THE COMMANDER:

Plans Office

UNCLASSIFIED

SECURITY CLASSIFICATION OF THIS PAGE (When Data Entered)

REPORT DOCUMENTATION PAGE

READ INSTRUCTIONS BEFORE COMPLETING FORM

1. REPORT NUMBER	2. GOVT ACCESSION NO.	3. RECIPIENT'S CATALOG NUMBER
RADC-TR-77-83		Scientific-2

4. TITLE (and Subtitle)

THE BEVERAGE WAVE ANTENNA: RADIATION FIELD PATTERNS

5. TYPE OF REPORT & PERIOD COVERED

Scientific Report No. 2

6. PERFORMING ORG. REPORT NUMBER

7. AUTHOR(s)

Robert M. Sorbello

8. CONTRACT OR GRANT NUMBER(s)

F19628-76-C-0057, and Joint Services Electronics Program Contract N00014-75-C-0648

9. PERFORMING ORGANIZATION NAME AND ADDRESS

Gordon McKay Laboratory, Harvard University
Division of Engineering and Applied Physics
Cambridge, Mass. 02138

10. PROGRAM ELEMENT, PROJECT, TASK AREA & WORK UNIT NUMBERS

61102F
5635-06-01

11. CONTROLLING OFFICE NAME AND ADDRESS

Deputy for Electronic Technology (RADC/ETER)
Hanscom AFB, MA 01731
Contract Monitor: John F. McIlvenna

12. REPORT DATE

February 1977

13. NUMBER OF PAGES

76

14. MONITORING AGENCY NAME & ADDRESS (if different from Controlling Office)

73 p.

15. SECURITY CLASS. (of this report)

UNCLASSIFIED

15a. DECLASSIFICATION/DOWNGRADING SCHEDULE

16. DISTRIBUTION STATEMENT (of this Report)

Approved for public release; distribution unlimited.

17. DISTRIBUTION STATEMENT (of the abstract entered in Block 20, if different from Report)

18. SUPPLEMENTARY NOTES

19. KEY WORDS (Continue on reverse side if necessary and identify by block number)

horizontal-wire antennas over an imperfectly conducting half-space
Beverage wave antennas
surface- and space-wave radiation patterns
theoretical analysis; exact antenna current expression
experimental measurements

20. ABSTRACT (Continue on reverse side if necessary and identify by block number)

This report presents the results of a theoretical and experimental investigation of the transmitting and receiving properties (far-field radiation patterns) of horizontal-wire antennas placed over an imperfectly conducting half-space. Particular emphasis is given to the Beverage wave antenna, a special type of horizontal-wire antenna placed in close proximity to the earth. Early work by Sommerfeld showed that the radiation from a dipole above an imperfect earth could be separated into a space wave (which could reflect off the iono-

DD FORM 1 JAN 73 1473 EDITION OF 1 NOV 65 IS OBSOLETE

UNCLASSIFIED

SECURITY CLASSIFICATION OF THIS PAGE (When Data Entered)

154000

20. ABSTRACT (Continued)

sphere and which predominates at large distances above the earth) and a surface wave (which could diffract around the curvature of the earth and which dominates close to the surface). Because of the difficulties involved in solving the Sommerfeld integral formulation, asymptotic approximations valid in the radiation zone have generally been employed to solve this problem. The useful approximate forms developed earlier by Norton have been used in this study, the only difference being that in the present analysis the exact expressions for the antenna current are used rather than an assumed current distribution. An expression for the space-wave radiation pattern is formulated using a "geometric optics" approximation, while the superposition principle is used to sum the fields of individual infinitesimal dipoles to obtain the surface-wave radiation pattern. Expressions for a number of useful antenna parameters (efficiency, front-to-back ratio, antenna gain, effective length) are then derived. A series of experimental measurements were made to verify the accuracy of the approximate theoretical formulation. Measurements were made to determine how the antenna spacing and the properties of the half-space affect the radiation patterns of Beverage wave antennas. Surface-wave radiation patterns were measured for Beverage antennas placed over fresh water and dry earth at heights ranging from $.01\lambda_0$ to $.25\lambda_0$. The measurements also served to verify that the asymmetrically driven, modified Beverage antenna can be used to obtain unidirectional surface-wave and space-wave radiation patterns equivalent to the radiation patterns of the conventional Beverage antenna.

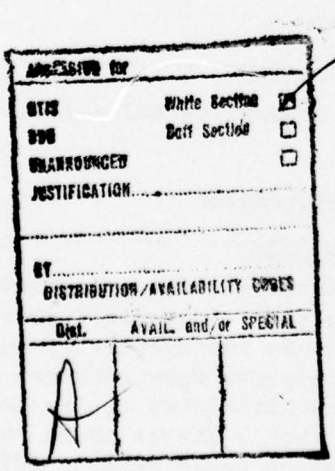

TABLE OF CONTENTS

PART I

ANALYTIC CONSIDERATIONS

1.1. Introduction

Probably the most important property of an antenna from the engineer's point of view is its radiation pattern. The purpose of an antenna in any communication system is to transmit or receive effectively a sufficient amount of energy in or from a desired direction. The far field or radiation pattern contains all information concerning the directional properties of only those field components sustained at far distances from the radiating source. Due to the Rayleigh-Carson reciprocal theorem [1], the transmitted and received radiation patterns are identical and, therefore, knowledge of the radiated pattern provides important additional information on the receiving properties of the antenna.

When considering the far-field characteristic of antennas in the presence of an imperfectly conducting half-space, a logical and fundamental starting point is to investigate the radiation properties of the infinitesimal electric dipole. As mentioned in Part I of [2], the classic Sommerfeld problem [3] derives the solutions for the electromagnetic fields of a dipole over a flat earth. The complexity of this solution has led to numerous misunderstandings as to the actual radiation mechanism involved. The original paper by Sommerfeld in 1909 [4] showed that the radiation from a dipole above an imperfect earth could be separated into a space or sky wave which could reflect off the ionosphere and a surface or ground wave which could diffract around the curvature of the earth, as shown in Fig. 1.1. The surface wave generated considerable interest especially for its use in radio transmission. Due to a minus sign error in Sommerfeld's original paper, anomalies such as "negative attenuation" and dips to zero in the surface-wave field intensity were predicted at finite distances from the dipole [5], [6]. Further questions were raised as to whether the Sommerfeld surface wave was indeed a Zenneck-type surface wave, i.e., a wave supported along a plane infinite interface which is exponentially attenuated in the direction of propagation along the interface and vertically upward and downward from the interface. Subsequent reformulation of the problem by Sommerfeld in 1926 [7] along with independent approaches by Weyl [8] and Van der Pol et al. [9] led to the

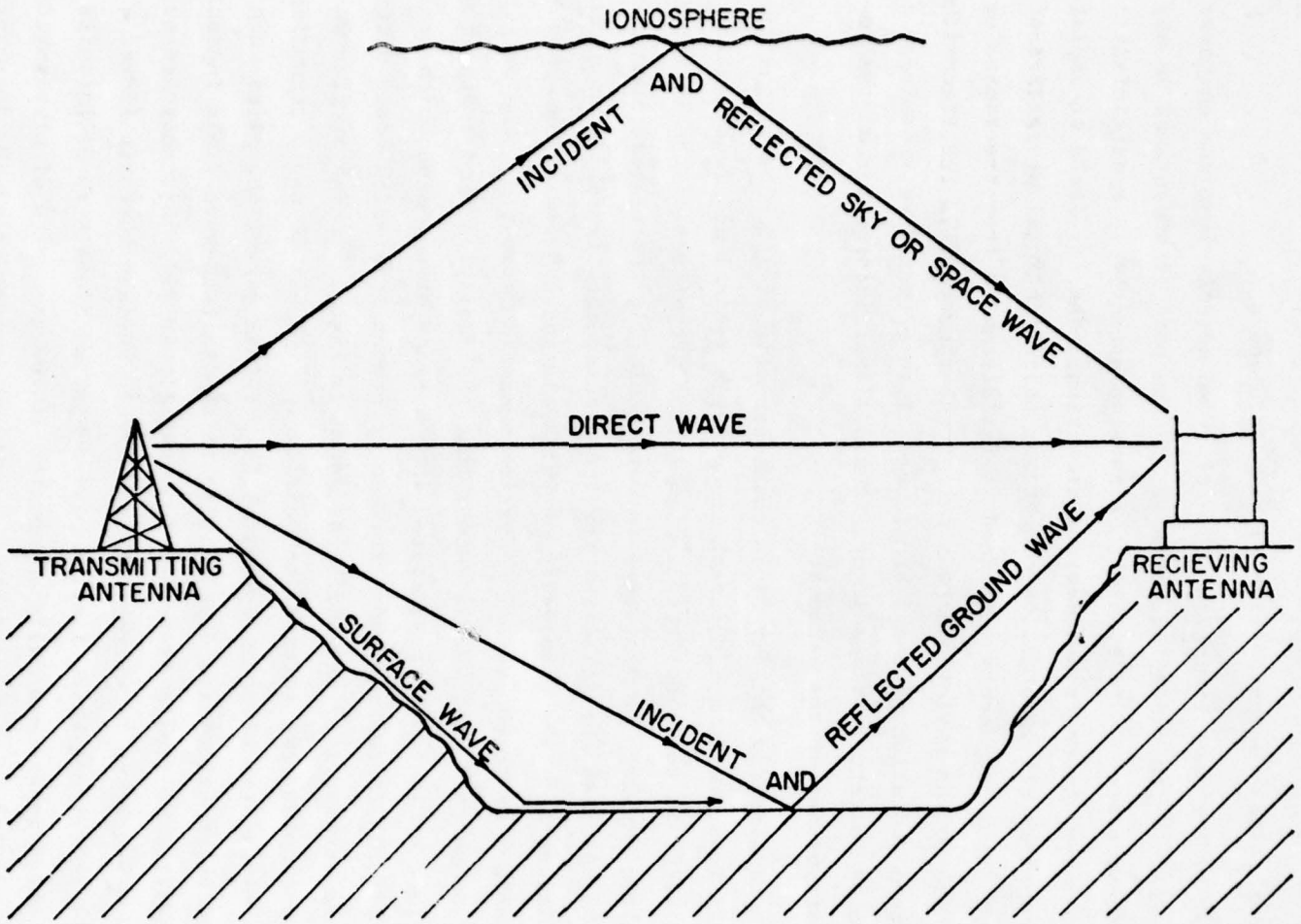

FIG. 1.1. POSSIBLE MECHANISMS OF TRANSMISSION FOR ANTENNAS OR ELEMENTARY SOURCES PLACED CLOSE TO THE EARTH.

discovery of the original sign error. Norton [10] later showed that this error in sign was responsible for the anomalies in the surface-wave attenuation factor observed by Sommerfeld and Rolf. Wise [11] and Burrows [12] reconfirmed the field decomposition into surface and space waves and further showed that the surface wave does not obey the requirements of a Zenneck surface wave.

Since antennas of finite length can be viewed as a summation of infinitesimal dipoles, it can be expected that a similar surface-wave and space-wave decomposition will occur for their radiation fields. The variation in the magnitude and phase for each dipole will determine the directional properties of the surface and space waves. This, of course, is reflected in the actual current distribution that exists on the wire antenna. With exact current expressions for the horizontal wire and Beverage antenna available [2, eqs. (1.6) and (1.64)], one can obtain the radiation pattern for these antennas by integrating Sommerfeld's original field expression for a dipole where $P_{\ell 1} = -j(I\, d\vec{\ell}/\omega)$. Due to difficulties concerning the Sommerfeld integrals [2], this problem is usually avoided by replacing the integrals with asymptotic approximations that are valid in the radiation zone. One of the more useful approximate forms for engineering use has been developed by Norton [13]. This formulation will provide the basis for the present development concerning far-field expressions for wires over a half-space and for the Beverage wave antenna. This approach has been used many times before, the only difference being that this time the exact expressions for the antenna current will be used rather than an assumed current distribution.

1.2. Asymptotic Development of Norton

Sommerfeld initially showed that the boundary-value problem associated with a horizontal dipole above an imperfect earth requires two components of the vector potential in order that all components of the field could be matched at the air-earth interface [3]. For a unit horizontal dipole parallel to the x axis (Fig. 1.2), two components of the Hertzian potential, Π_x^h and Π_z^h, are necessary. The electric field in air associated with these potentials is:

$$\vec{E} = [k_1^2 \vec{\Pi} + \vec{\nabla}\vec{\nabla} \cdot \vec{\Pi}] \tag{1.1}$$

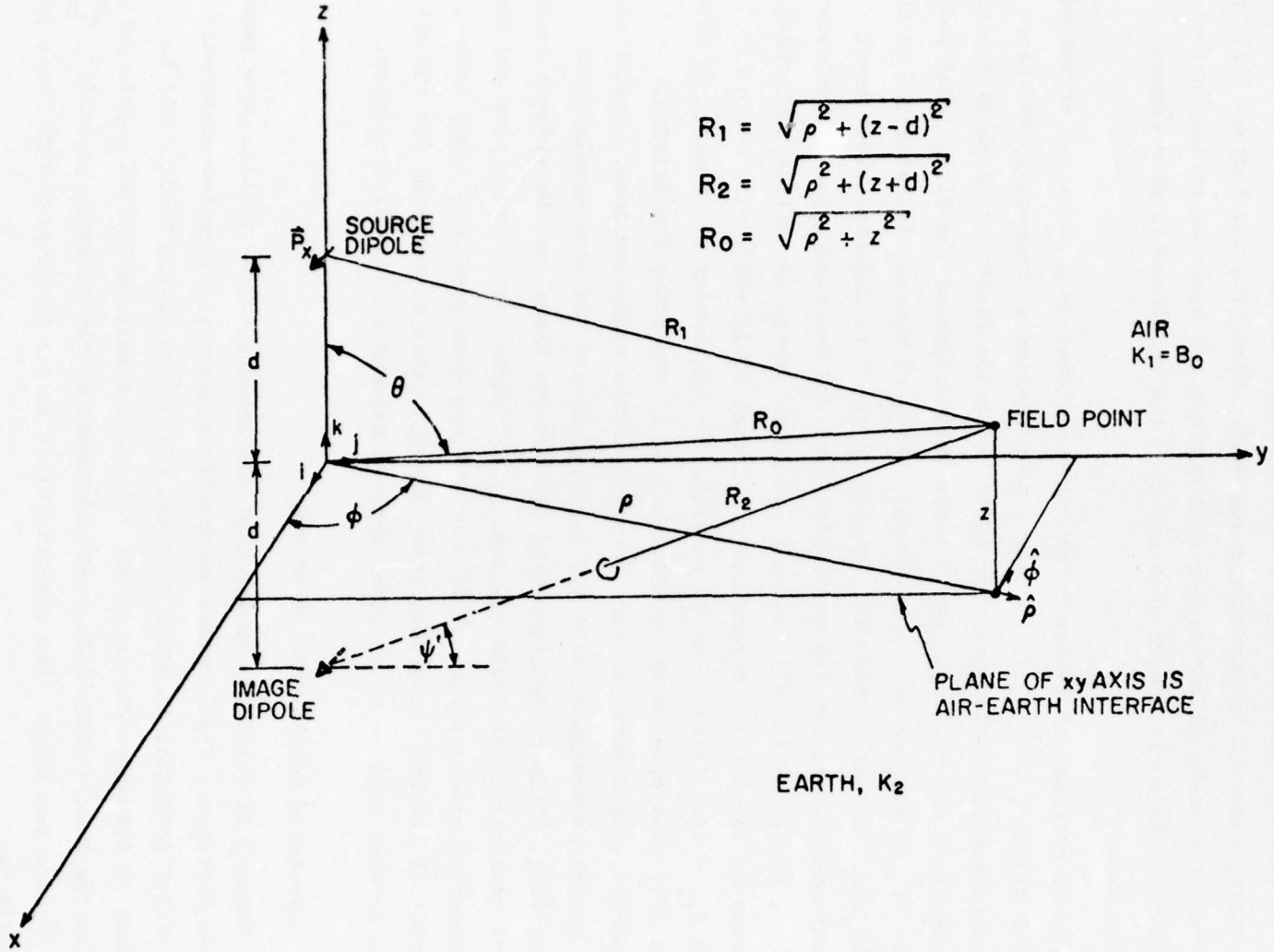

FIG. 1.2. GEOMETRY FOR HORIZONTAL ELECTRIC DIPOLE FIELD PATTERNS

where Sommerfeld and others have shown that

$$\vec{\Pi} = \Pi_x^h \hat{i} + \Pi_z^h \hat{k} \tag{1.2}$$

The two components of the Hertzian potential are:

$$\Pi_x^h = \frac{\vec{P}_{x1}}{4\pi\epsilon_1}\left(-\frac{e^{-jk_1R_1}}{R_1} + \frac{e^{-jk_1R_2}}{R_2} - H\right) \tag{1.3}$$

with

$$H = \int_0^\infty \frac{2}{\ell + m} J_0(\lambda\rho)e^{-(d+z)\ell}\ \lambda\ d\lambda \tag{1.4}$$

and

$$\Pi_z^h = -\frac{\vec{P}_{x1}\cos\phi}{4\pi\epsilon_1}\int_0^\infty \frac{2(1-u^2)}{(\ell + m)(\ell + u^2m)} J_0'(\lambda\rho)e^{-(d+z)\ell}\ \lambda\ d\lambda \tag{1.5}$$

with

$$\ell^2 = \lambda^2 - k_1^2 \tag{1.6a}$$

$$m^2 = \lambda^2 - k_2^2 \tag{1.6b}$$

$$u = k_1/k_2 \tag{1.6c}$$

All other quantities are adequately defined in Fig. 1.2. The integrals in (1.4) and (1.5) are the Sommerfeld integrals that have been the subject of considerable investigation.

Wise [15] has shown that it is possible to express the electric-field components of the horizontal dipole as:

$$E_z^h = \vec{Q}\cos\phi\ \frac{\partial^2}{\partial\rho\partial z}\left(V - \frac{e^{-jk_1R_1}}{R_1} - \frac{e^{-jk_1R_2}}{R_2}\right) \tag{1.7a}$$

$$E_\rho^h = \vec{Q}\cos\phi\left[\frac{\Pi_x^h k_1^2}{\vec{Q}} - \frac{\partial^2}{\partial\rho^2}\left(\frac{e^{-jk_1R_1}}{R_1} - \frac{e^{-jk_1R_2}}{R_2} + u^2V\right)\right] \tag{1.7b}$$

$$E_{\phi}^{h} = \vec{Q} \sin\phi \left[\frac{\Pi_{x1}^{h} k_1^2}{\vec{Q}} - \frac{1}{\rho} \frac{\partial^2}{\partial \rho^2} \left(\frac{e^{-jk_1 R_1}}{R_1} - \frac{e^{-jk_1 R_2}}{R_2} + u^2 V \right) \right] \tag{1.7c}$$

where

$$\vec{Q} = -\vec{P}_{x1}/4\pi\epsilon_1 \tag{1.8a}$$

$$V = \int_0^{\infty} \frac{2}{\ell + u_m^2} J_0(\lambda\rho) e^{-(d+z)\ell} \lambda \, d\lambda \tag{1.8b}$$

The V integral appears in the solution for the Hertz potential of a vertical electric dipole. The advantage of (1.7) is that the fields are now expressed in terms of two similar integrals, V and H, and the more complicated integral associated with Π_z^h has been eliminated. The V and H integrals are the starting points for much of the asymptotic work done to date.

Van der Pol was able to take the expressions for V and H and express them in the following approximate form:

$$V \doteq 2 \left(\frac{e^{-jk_1 R_2}}{R_2} - jk_2 \int_0^{\infty} \frac{e^{-jk_1 (R' + s/u)}}{R'} ds \right) \tag{1.9a}$$

$$H \doteq 2 \left(\frac{e^{-jk_1 R_2}}{R_2} - jk_2 \int_0^{\infty} \frac{e^{-jk_1 (R'' + s/u)}}{R''} ds \right) \tag{1.9b}$$

where

$$R'^2 \doteq \rho^2 + (d + z + s/u^2)^2 \tag{1.10a}$$

$$R''^2 \doteq \rho^2 + (d + z + s)^2 \tag{1.10b}$$

The major assumption involved in this approximation is that medium two be sufficiently conducting to assure that α_2 is large enough to provide a rapid decrease with radial distance. With this assumption the above approximate forms for R' and R'' can be obtained along with the simplification of a *radial integration*. A precise statement of the condition is:

$$\alpha_2 R_2 >> 1 \quad \text{or} \quad R_2 >> d_s \tag{1.11}$$

where d_s is the skin depth. King [14] has shown that this assumption is usually less restrictive than the conventional far-zone conditions, $\beta_1 R_1 >> 1$, and can be shown to hold for a wide range of media.

Norton's formulation [13] begins with the approximate integrals of Van der Pol, equations (1.9a,b) for the V and H functions. Norton starts by using reasoning similar to that of Van der Pol to simplify the s integration. Specifically, if α_2 is large enough, then the principal contribution to the integrals will come only when s is small. Accordingly, (1.10a) may be expanded in a Taylor series as follows:

$$R'(s) = R'(0) + s\left[\frac{\partial R'(s)}{\partial s}\right]_{s=0} + \frac{s^2}{2}\left[\frac{\partial^2 R'(s)}{\partial s^2}\right]_{s=0} + \ldots$$

With this equation, (1.10a) can be further approximated as:

$$R'(s) \doteq R_2 + \frac{(d+z)s}{R_2 u^2} + \frac{s^2}{2R_2 u^4} \tag{1.12}$$

By substituting (1.12) into the V integral, (1.9a) leads to the following:

$$V \doteq 2\,\frac{e^{-jk_1 R_2}}{R_2}\left\{1 - jk_2 \int_0^\infty e^{-jk_1[(d+z)s/R_2u^2 + s/u + s^2/2R_2u^4]}\right\} \tag{1.13}$$

With the following identity

$$\int_0^\infty e^{a^2 s^2 + bs}\, ds = -j\,\frac{\pi^{1/2}}{2a}\, e^{-b^2/4a^2}\, \mathrm{erfc}[j(b^2/4a^2)^{1/2}] \tag{1.14}$$

where

$$\mathrm{erfc}(x) = (2/\pi^{1/2}) \int_x^\infty e^{-u^2}\, du$$

an approximate expression for V may be written as:

$$V \doteq 2\,\frac{e^{-jk_1 R_2}}{R_2}\left[1 - j(\pi p')^{1/2}\, e^{-w'}\, \mathrm{erfc}(jw'^{1/2})\right] \tag{1.15}$$

where

$$p' = -j\frac{k_1 R_2 u^2}{2} \tag{1.16a}$$

$$w' = p[1 + (d + z)/uR_2]^2 \tag{1.16b}$$

Norton's next step was to expand the erfc function for large argument and compare the results with an exact asymptotic formulation by Wise [15]. The comparison is as follows:

$$\text{Norton:}\quad V \doteq \frac{2e^{-jk_1R_2}}{R_2}\left\{1 - [1 + (d + z)/uR_2]^{-1}\left(1 + \frac{1}{2w'}\right)\right\} \quad \text{for } |w'| > 20 \tag{1.17}$$

$$\text{Wise:}\quad V \doteq \frac{2e^{-jk_1R_2}}{R_2}\{1 - [1 + \sin\psi'/u(1 - u^2\cos^2\psi')^{1/2}]^{-1}\} \quad \text{where } \sin\psi' \equiv (z + d)/R_2 \tag{1.18}$$

It is evident that for sufficiently large values of w', (1.17) is equivalent to (1.18) except for the 1/u term which must be multiplied by the factor $(1 - u^2\cos^2\psi')^{1/2}$. Due to the condition placed on α_2 in Van der Pol's work, Norton's development implicitly assumed that $|u^2| << 1$.

If it is noted that even for dry earth with $\varepsilon_r = 5$, $|u^2|$ is less than .2 for all frequencies, it can be easily seen that with restriction (1.11) the $(1 - u^2\cos^2\psi')^{1/2}$ factor is nearly unity and, thus, the two results agree quite well. In order to obtain a single formula that is useful for all values of u subject to the condition $\beta_1 R_2 >> 1$ and for $|u^2| << 1$ subject to the restriction that $\alpha_1 R_2 >> 1$, Norton arbitrarily introduces the factor $(1 - u^2\cos^2\psi')^{1/2}$ into the general integral (1.13) as follows:

$$V \doteq 2\frac{e^{-jk_1R_2}}{R_2} - jk_2(1 - u^2\cos^2\psi')^{1/2}\int_0^\infty \frac{e^{-jk_1[R' + s(1 - u^2\cos^2\psi'/u)^{1/2}]}}{R'}\,ds \tag{1.19}$$

There appears to be no rigorous justification for the inclusion of this factor except to obtain agreement with Wise's formulation, yet it does lead to some interesting and useful results. By expanding R' as in (1.12),

substituting into (1.19), and utilizing the identity in (1.14), Norton obtained the final form for V as:

$$V \doteq [(1 - R_v)F + 1 + R_v] \frac{e^{-jk_1R_2}}{R_2} \tag{1.20}$$

where

$$R_v = \frac{\sin \psi' - u(1 - u^2 \cos^2 \psi')^{1/2}}{\sin \psi' + u(1 - u^2 \cos^2 \psi')^{1/2}} \tag{1.21}$$

$$F = 1 - j(\pi w)^{1/2} e^{-w} \operatorname{erfc}(jw^{1/2}) \tag{1.22}$$

$$w = 4p_1/(1 - R_v)^2 \tag{1.23}$$

$$p_1 = -jk_1R_2u^2(1 - u^2 \cos^2 \psi')/2 \equiv pe^{-b} \tag{1.24}$$

By following similar procedures and arguments the H function can be evaluated to give:

$$H \doteq [(1 + R_h)G + 1 - R_h] \frac{e^{-jk_1R_2}}{R_2} \tag{1.25}$$

where

$$R_h = \frac{u \sin \psi' - (1 - u^2 \cos^2 \psi')^{1/2}}{u \sin \psi' + (1 - u^2 \cos^2 \psi')^{1/2}} \tag{1.26}$$

$$G = [1 - j(\pi v)^{1/2} e^{-v} \operatorname{erfc}(jv^{1/2})] \tag{1.27}$$

$$v = 4q_1/(1 + R_h)^2 \tag{1.28}$$

$$q_1 = -jk_1R_2(1 - u^2 \cos^2 \psi')/2u^2 \equiv -qe^{jb'} \tag{1.29}$$

With formulas developed for H and V that are valid in the far zone, the far-zone electromagnetic fields can be evaluated readily using (1.1). This involves essentially nothing more than numerous partial differentiations. After performing the indicated manipulations, Norton was able to cast the

radiation field of a horizontal dipole at a height d above the earth (Fig. 1.3) into the following form:

$$E^h_{space} = \frac{k_1^2 \vec{P}_{xl}}{4\pi\varepsilon_1} \frac{e^{-jk_1(R_0 - d\sin\psi)}}{R_0} [\cos\phi \sin\psi (1 - R_v) e^{-2jk_1 d \sin\psi} \hat{\psi}$$

$$+ \sin\phi (1 + R_h) e^{-2jk_1 d \sin\psi} \hat{\phi} \qquad (1.30)$$

$$E^h_{surface} = \frac{k_1^2 \vec{P}_{xl}}{4\pi\varepsilon_1} \frac{e^{-jk_1(R_0 + d\sin\psi)}}{R_0} \left\{ \cos\phi\, u(1 - u^2\cos^2\psi)^{1/2} \right.$$

$$\times (1 - R_v) F \left[\cos\psi \left(1 + \frac{\sin^2\psi}{2}\right) \hat{\psi} + u(1 - u^2\cos^2\psi)^{1/2} \right.$$

$$\left. \left. \times \left(\frac{1 - \sin^4\psi - \dfrac{(1 - R_h)G}{(1 - R_v)u^2 F}}{1 - u^2\cos^2\psi} \right) \hat{\rho} \right] + \sin\phi (1 - R_h) G \hat{\phi} \right\} \qquad (1.31)$$

for $R >> \lambda$

where R_v, F, R_h and G are given in (1.21), (1.22), (1.26) and (1.27). Note that in the far zone the following approximations are used:

$$R_1 \approx R_2 \times R_0 \quad \text{and} \quad \psi' \approx \psi = 90° - \theta$$

The final expressions (1.30) and (1.31) will be used subsequently to develop far-field expressions for finite wires over the ground. First, however, it is instructive to note the important conclusions that can be drawn from these two equations:

1) The decomposition of the radiation field into surface-wave and space-wave components agrees with previous formulations by Sommerfeld and others. The space wave predominates at large distances above the earth, while the surface wave is dominant at the surface of the earth where the space wave is negligible.

2) For the surface wave at large distances, $|w| > 20$, it can be shown that $G \approx u^2 F$ asymptotically. Substituting this approximation into (1.31)

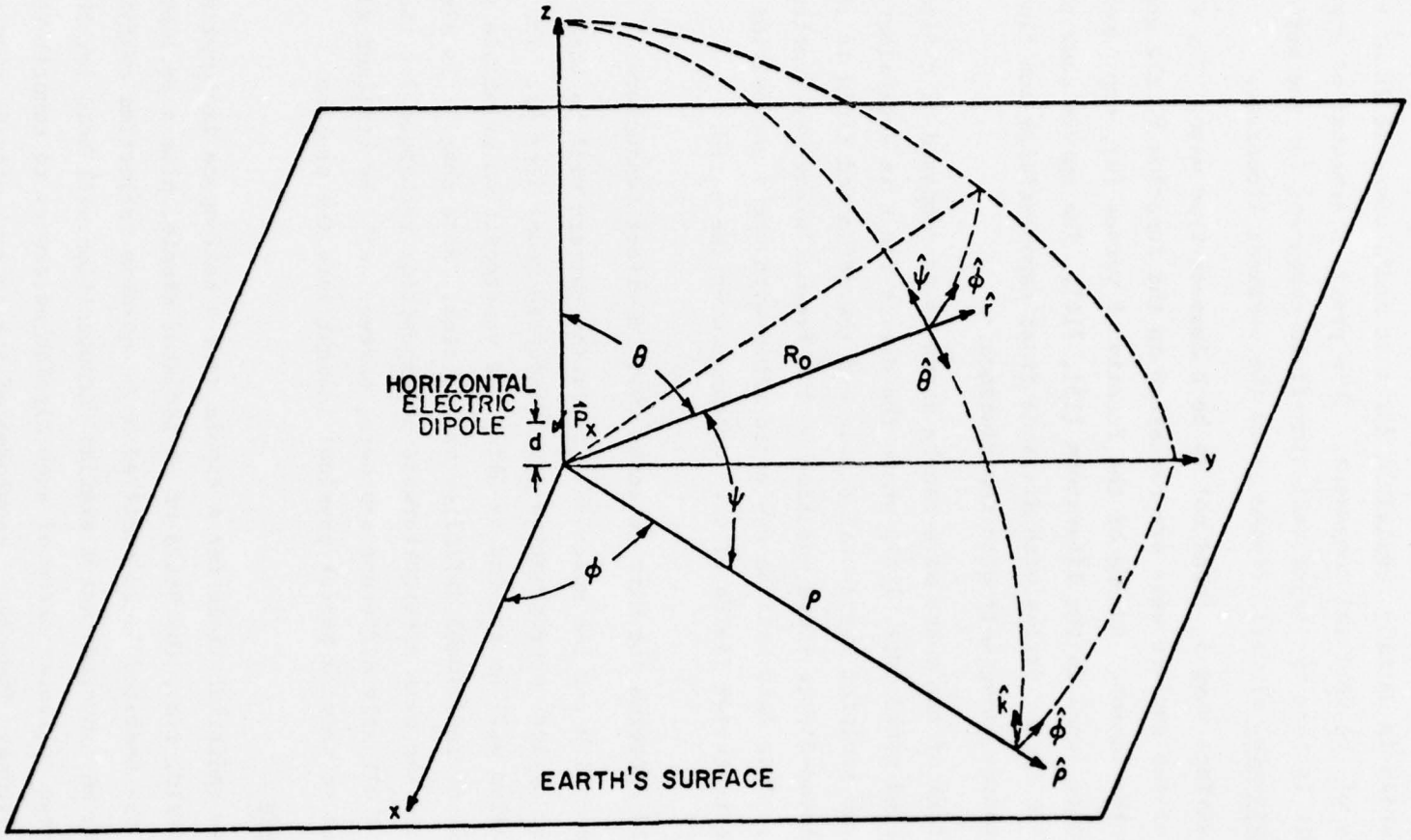

FIG. 1.3. FAR ZONE COORDINATES FOR HORIZONTAL DIPOLE ABOVE THE EARTH.

gives the result that the electric vector in the surface wave at $\psi = 0$ is predominantly in the vertical $\hat{k}$ direction. There is also a small horizontal $\hat{\phi}$ component which is usually negligible for most media since it is u^3 times the intensity of the vertical component. This provides somewhat of a surprising result in that the major radiation-field component for the surface wave of a horizontal electric dipole is in the vertical direction.

3) The surface wave is found not to be a Zenneck-type wave. The characteristics of the surface wave are contained in the function F, the ground-wave attenuation factor. Curves of the function F versus $|w|$, the numerical distance, can be found in the literature [13], [14]. The curves show that the attenuation factor varies with distance first exponentially and finally, at large distances, inversely with the distance.

4) The form of the space wave can be shown to be composed of a direct plus a reflected field (Fig. 1.1), where the direct field is equivalent to the field of an isolated horizontal dipole and the reflected field is the incident isolated-dipole field modified by the Fresnel plane-wave reflection coefficients. This fact will be exploited along with the superposition to solve for the radiation fields of wire antennas over the earth.

1.3. Far-Field Patterns for Wire Antennas Over Imperfect Conductors

The formulation for the space-wave radiation pattern will be based on the "geometric optics" approximation just discussed under item 4). The surface-wave problem will be treated by using the superposition principle to sum the fields of individual infinitesimal dipoles. Note that it is also possible to use the same straightforward superposition technique for the space wave. A slightly different approach, however, will be utilized since it is believed to provide better physical insight into the problem.

Space Wave

Since the radiation field for a dipole over a half-space is comprised of a direct field, i.e., the field of an isolated dipole, plus a reflected field, i.e., the isolated field modified by plane-wave reflection coefficients, it can be expected that a similar decomposition will hold for the infinitely large collinear array of such dipoles necessary to constitute a finite wire antenna. Therefore, knowledge of the current distribution that

exists on a wire antenna would be sufficient to evaluate the radiated fields. The electromagnetic field for any radiating source surrounded by medium k_1 can be expressed as:

$$\vec{E} = -(j\omega/k_1^2)(\vec{\nabla}\vec{\nabla} \cdot \vec{A} + k_1^2\vec{A}) \tag{1.32a}$$

$$\vec{B} = \vec{\nabla} \times \vec{A} \tag{1.32b}$$

where

$$\vec{A} = \frac{1}{4\pi\nu_1} \int_\tau \rho_m^{\rightarrow} v' \frac{e^{-jk_1R}}{R} d\tau' + \int_\Sigma \eta_m^{\rightarrow} v' \frac{e^{-jk_1R}}{R} d\sigma' \tag{1.33}$$

The current distributions for the source are defined by $\rho_m^{\rightarrow} v$ and $\eta_m^{\rightarrow} v$ which are the essential density functions for volume and surface currents. $R = [(x - x')^2 + (y - y')^2 + (z - z')^2]^{1/2}$ is the distance between the source point (primed coordinates) and the field point (unprimed coordinates).

Consider the case of a thin cylindrical wire ($\beta_0 a << 1$) of half-length h and radius a, placed along the s axis and center-driven by a slice generator such that an axial current I(s') exists along the wire (Fig. 1.4). The radiation zone for the wire is defined by:

$$\beta_1 R >> 1 \tag{1.34a}$$

$$R >> h \tag{1.34b}$$

Subject to the above conditions, (1.33) reduces in the radiation zone to the following form [1]:

$$\vec{A}^r = \hat{s}A_s^r \quad , \quad A_s^r = \frac{\hat{s}}{4\pi\nu_1} \frac{e^{-jk_1R_0}}{R_0} \int_{-h}^{h} I(s')e^{jk_1(\hat{R}_0 \cdot s')} ds' \tag{1.35}$$

where for large distances $R \approx R_0$ in the denominator of (1.33) and $R \approx R_0 - (\hat{R}_0 \cdot s)$ in the phase term since distances on the wire may not be small compared to a wavelength. For a cylindrical antenna placed along the s axis it can be shown [1] that in the far zone the field decreases inversely as the radial distance, while the energy propagates in the $\hat{R}_0$ radial direction.

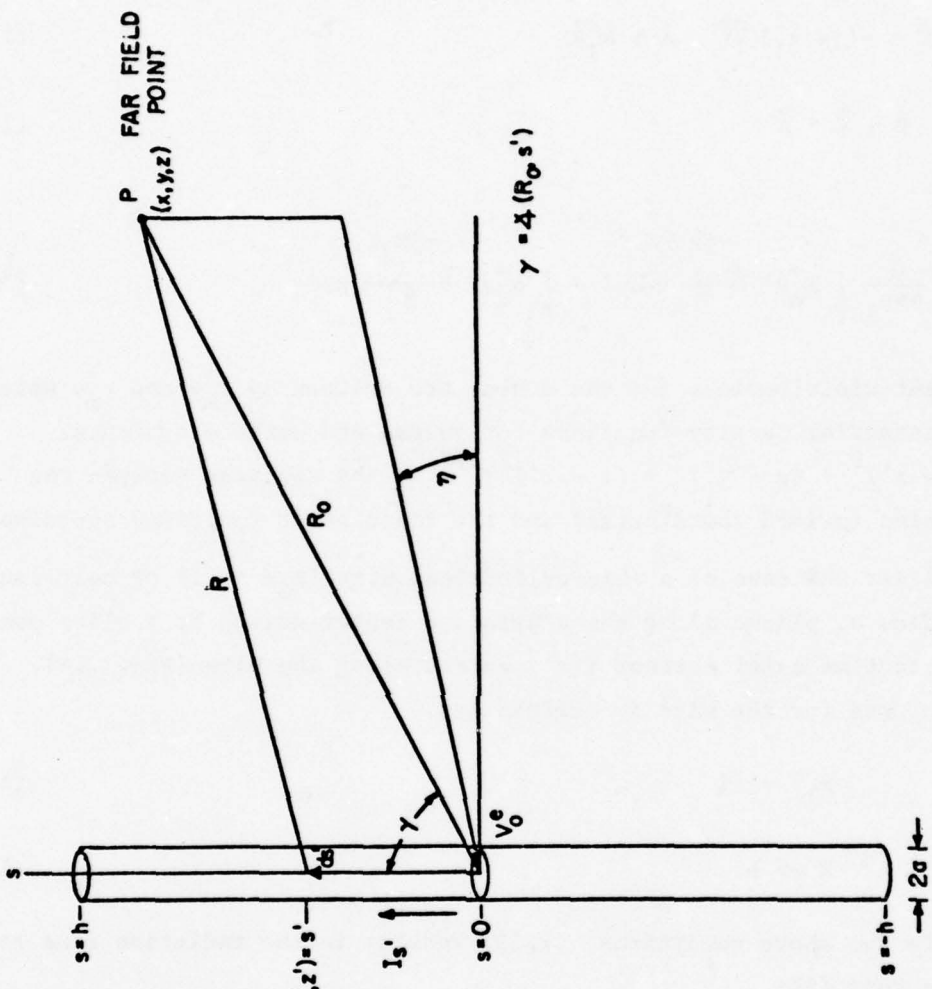

FIG. 1.4. CENTER DRIVEN CYLINDRICAL ANTENNA AND FAR ZONE COORDINATES

Due to the spherical-wave nature of the field, there are no components in the radial direction and, therefore, the electric field can be expressed as:

$$E^r = -j\omega(\hat{\theta}A_\theta^r + \hat{\phi}A_\phi^r) \tag{1.36}$$

Substituting (1.35) into (1.36) and decomposing the current vector into $\hat{\theta}$ and $\hat{\phi}$ components give

$$E^r = -\frac{j\omega}{4\pi\nu_1}\frac{e^{-jk_1R_0}}{R_0}\{\hat{\theta}\int I_\theta(s')e^{jk_1(\hat{R}\cdot s')}ds' + \hat{\phi}\int I_\phi(s')e^{jk_1(\hat{R}\cdot s')}ds'\} \tag{1.37}$$

This is the complete far-zone expression for the electric field of an isolated wire antenna in medium k_1.

In Fig. 1.5 a cylindrical wire of radius a and half-length h directed along the x axis has been displaced a distance d above the origin. It is now assumed that medium one is free space and that the wire is completely isolated from all other sources. From Fig. 1.5 it can be seen that R', the distance from the source to the field point, contains an added factor due to the shift of the antenna from the origin. Specifically, it is graphically shown that:

$$R' \approx R_0 - (\hat{R}\cdot s') - d\cos\theta \tag{1.38}$$

With the total antenna current directed along the x axis, the following decomposition can be obtained:

$$I_T(x') = \hat{x}I_x(x') = \hat{\theta}I_\theta(x') + \hat{\phi}I_\phi(x')$$

where

$$I_\theta(x') = I_x(x')\hat{\theta}\cdot\hat{x} = I_x(x')(\hat{x}\cos\phi\cos\theta + \hat{y}\sin\phi\cos\theta - \hat{z}\sin\theta)\cdot\hat{x}$$

$$= I_x(x')\cos\theta\cos\phi \tag{1.39}$$

and

$$I_\phi(x') = I_x(x')\hat{\phi}\cdot\hat{x} = I_x(x')[(\hat{y}\cos\phi - \hat{x}\sin\phi)\cdot\hat{x}] = -I_x(x')\sin\phi \tag{1.40}$$

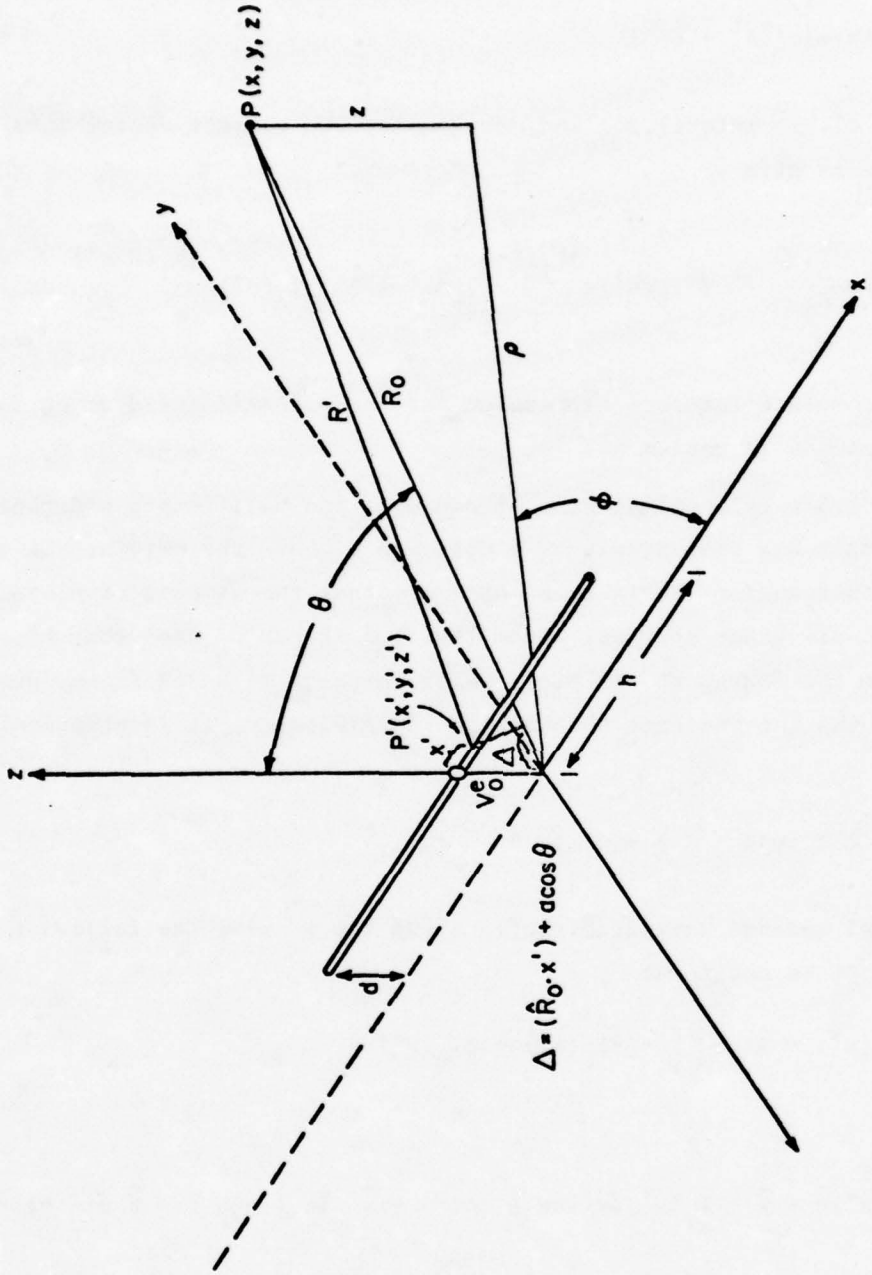

FIG. 1.5. COORDINATES FOR CYLINDRICAL ANTENNA HORIZONTALLY DISPLACED ABOVE PLANE OF xy AXIS.

If it is noted that $(\hat{R} \cdot s') = (\hat{R} \cdot x') = x' \cos\phi \sin\theta$, the expression for the radiation field can be obtained by substituting (1.38) - (1.40) into (1.37). Performing these substitutions and employing the following change in constants

$$\omega/v_0 = \beta_0\zeta_0 \quad , \quad \zeta_0 = 120\pi \text{ ohms}$$

one obtains

$$E^r = \frac{-j30\beta_0}{R_0} e^{-j\beta_0 R_0 + \beta_0 d \cos\theta} [-\hat{\phi} \sin\phi \int_{-h}^{h} I_x(x') e^{j\beta_0 \cos\phi \sin\theta x'} dx'$$

$$+ \hat{\theta} \cos\phi \cos\theta \int_{-h}^{h} I_x(x') e^{j\beta_0 \cos\phi \sin\theta x'} dx'] \quad (1.41)$$

Consider now the case in which the region $z \leq 0$ is no longer air but is filled with an imperfectly conducting material such as earth with parameters ϵ_{r2}, σ_2. With hindsight obtained from the previous development by Norton, it can be shown that two effects are involved in modifying the radiation field due to the interface. First of all, the proximity of the earth to the wire modifies the current distribution, as shown in [2]. Secondly, a reflected field is now set up by the interface which must be combined with the direct isolated field to obtain the total radiation pattern. If the correct current distribution is known, (1.41) gives the proper expression for the direct field. To obtain the correct expression for the reflected field, it is necessary to examine what effect the polarization of the incident field will have on its reflection from a plane surface.

Figures 1.6a and 1.6b present the two types of polarization that can occur when a plane wave impinges upon a plane interface. The plane of incidence is defined as the plane containing the propagation vector and the normal to the interface at the point of reflection. For both cases in Fig. 1.6, the plane of the page represents the plane of incidence. The case in Fig. 1.6a is characterized by having the electric field perpendicular to the plane of incidence or horizontal to the reflecting surface. For this reason the case is often referred to as horizontal polarization. In Fig. 1.6b the electric field is parallel to or in the plane of incidence and is often

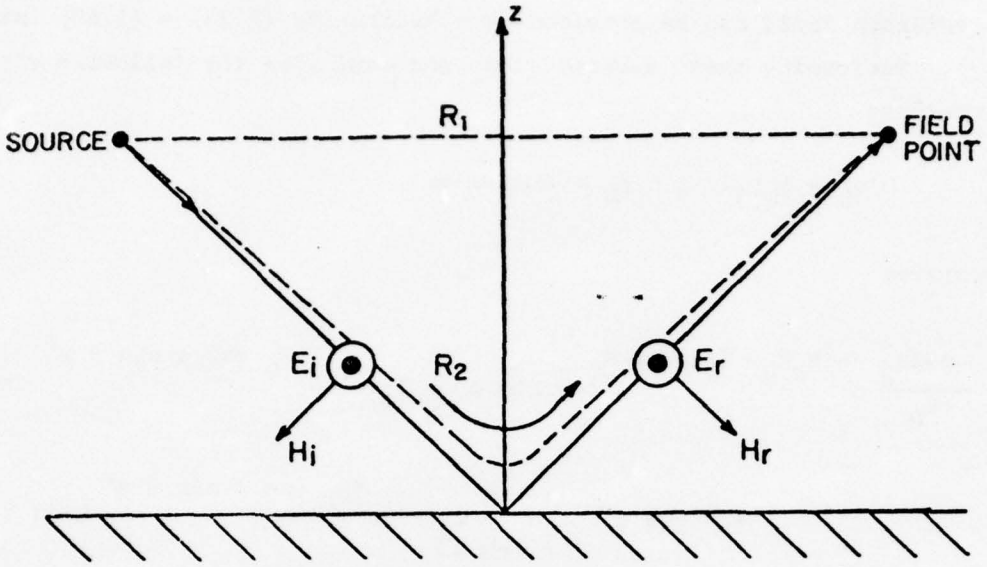

a) HORIZONTAL POLARIZATION

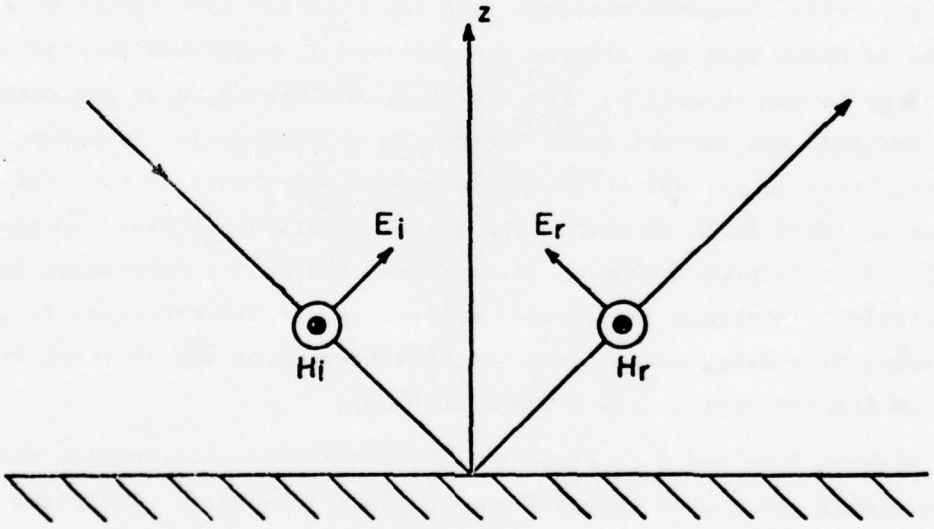

b) VERTICAL POLARIZATION

FIG. 1.6. WAVE REFLECTION OFF A PLANE INTERFACE

referred to as vertical polarization even though the electric vector may have components both horizontal and vertical to the interface.

For horizontal polarization it can be easily shown [16], [17] that

$$E_h = \text{total horizontal component} = E_i(r_1) + E_r(r_2)$$

$$= E_i(r_1) + R_h E_i(r_2) \tag{1.42}$$

where r_1 is the direct distance from the antenna-source point to the far-field point and r_2 represents the distance between the same points but through the reflecting path (Fig. 1.6). E_i and E_r are the direct and reflected vectors, respectively, and R_h is the Fresnel reflection coefficient given by (1.26). For the case of vertical polarization (polarization parallel to the plane of incidence) the total horizontal and total vertical components must be considered separately. When this is done, it is easy to show that

$$E_h' = \text{total horizontal component} = E_i(r_1) - R_v E_i(r_2) \tag{1.43}$$

$$E_v = \text{total vertical component} = E_i(r_1) + R_v E_i(r_2) \tag{1.44}$$

where R_v is the Fresnel coefficient for vertical polarization given by (1.21).

Figure 1.7 depicts the situation for a wire over a half-space, delineates the path for direct and reflected transmission, and shows the plane of incidence for the far-field components. It is apparent that E_ϕ is always perpendicular to the plane of incidence and, thus, can be categorized as horizontal polarization. With this fact it can be concluded that

$$E_{\phi T} = E_\phi^i(r_1) + R_h E_\phi^i(r_2) \tag{1.45}$$

On the other hand, it is evident that E_θ lies in the plane of incidence and, thus, represents a case of vertical polarization. It follows that it is necessary to decompose E_θ into vertical and horizontal components. Specifically, it can be shown that

$$E_\theta = E_\rho \cos\theta - E_z \sin\theta \tag{1.46}$$

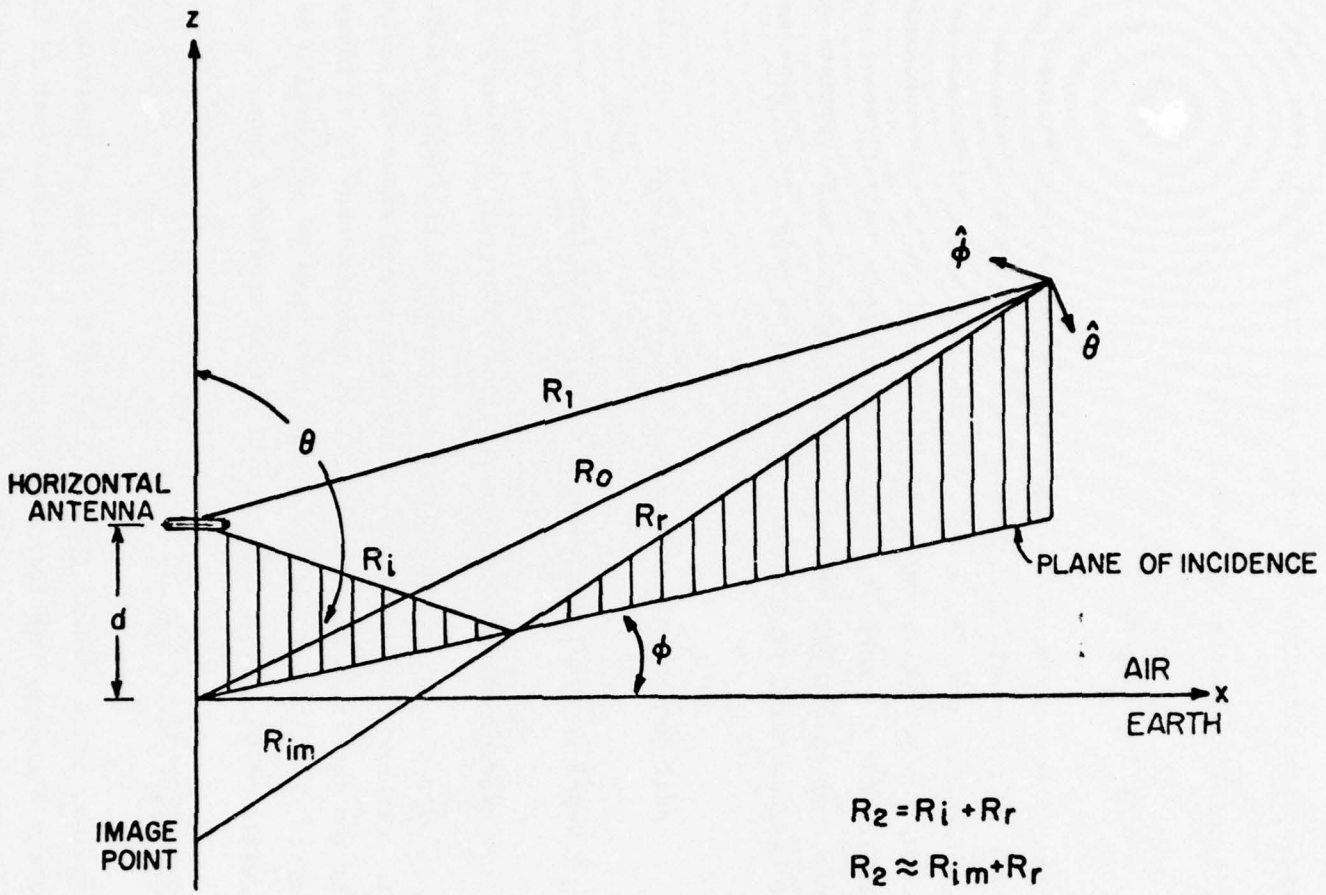

FIG. 1.7. DIRECT AND REFLECTED WAVE PROPAGATION FOR ANTENNA OVER THE EARTH.

where E_ρ is the total horizontal component and E_z is the total vertical component. Due to the fact that the current source is along the $\hat{x}$ direction, no electric-field component in the $\hat{z}$ direction is to be expected. Therefore, only the horizontal component is present and it follows from (1.43) that

$$E_{\theta T} = E_\theta^i(r_1) - R_v E_\theta^i(r_2) \tag{1.47}$$

Thus, the total electric field for a wire above a plane interface can be determined from (1.45) and (1.47) where E^i is contained in (1.41).

Previously it has been shown that for the direct wave

$$r_1 = R' \approx R_0 - (\hat{R} \cdot x') - d \cos\theta \tag{1.48a}$$

Similarly, the following approximation holds for the reflected wave:

$$r_2 \approx R_0 - (\hat{R} \cdot x') + d \cos\theta \tag{1.48b}$$

where r_2 is approximately equal to the distance from an image antenna at a point d below the interface. By using the standard far-field approximations with $r_1 = r_2 = R_0$ in the denominator and (1.48a,b) used in the exponent, the space wave can be written as:

$$E_{space} = \hat{\phi}\, j \frac{30\beta_0}{R_0} e^{-j(\beta_0 R_0 - \beta_0 d \cos\theta)} \sin\phi\, \bar{A}\, (1 + R_h e^{-j2\beta_0 d \cos\theta})$$

$$- \hat{\theta}\, j \frac{30\beta_0}{R_0} e^{-j(\beta_0 R_0 - \beta_0 d \cos\theta)} \cos\phi \cos\theta\, \bar{A}\, (1 - R_v e^{-j2\beta_0 d \cos\theta}) \tag{1.49}$$

where

$$\bar{A} = \int_{-h}^{h} I(x') e^{j\beta_0 \cos\phi \sin\theta\, x'}\, dx' \tag{1.50}$$

Surface Wave

In the procedure outlined above there is no way to acquire information concerning the surface wave. Naively setting $\theta = 90°$ in (1.49) shows that the space wave cancels at the interface. To obtain a suitable expression

for the surface-wave radiation pattern, it is necessary to superimpose the contributions of the individual infinitesimal dipoles from (1.31) that together comprise the total antenna length. This can be accomplished easily by replacing $\vec{P}_{x1}$ by its infinitesimal-element equivalent, $I\,dx/j\omega$, then substituting into (1.31), and integrating the response of each individual dipole. By using the same far-field approximations encountered in the space-wave development, the surface-wave radiation pattern can be written as:

$$E_{surface} = j\frac{30\beta_0}{R_0} e^{-j(\beta_0 R_0 + \beta_0 d\cos\theta)} \bar{A} \left\{ \cos\phi\,[u(1-u^2\cos^2\psi)^{1/2}] \right.$$

$$\times (1-R_v)F\left[\cos\phi\left(1+\frac{\sin^2\psi}{2}\right)\hat{\psi} + u(1-u^2\cos^2\psi)^{1/2}\right.$$

$$\left.\left.\times\left(\frac{1-\sin^4\psi - \dfrac{(1-R_h)G}{(1-R_v)u^2F}}{1-u^2\cos^2\psi}\right)\hat{\rho}\right] + \sin\phi\,(1-R_h)G\,\hat{\phi}\right\} \qquad (1.51)$$

with $\bar{A}$ given by (1.50) as before and

$$\psi = 90° - \theta$$

The quantities F, G, R_v and R_h are the same as have been applied previously to the dipole problem.

Note that this very simplistic procedure could also have been applied to the space wave and that the same expression as in (1.49) would have resulted. The approach that was taken proves to be more informative and more straightforward in developing the necessary $\bar{A}$ function.

Equations (1.49) and (1.51) constitute the geometric-optics approximation and have proven to be quite accurate for the radiation field. More exact field evaluation would necessitate more accurate approximations for the Sommerfeld integrals.

1.4. Field Calculations for Beverage and Wire Antennas

The calculation of the far-field pattern can now be accomplished by utilizing (1.49) and (1.51) along with a knowledge of the correct antenna

current. The difference between the calculation which follows and all previous work lies in the fact the correct antenna current can now be utilized, based on the developments presented and verified in Parts I and III of [2]. Except for multiplicative factors, the field calculations involve the evaluation of the $\bar{A}$ integral for the various current expressions developed in Part I of [2].

It has been shown [2, see Fig. 1.9] that for the asymmetrically loaded antenna placed above an imperfect ground the current is found to be:

$$I(x) = \begin{cases} A \sin k_L(s - x) + B \sin k_L(q + x) & 0 \leq x \leq \ell_1 \quad (1.52a) \\ A \sin k_L(s - x) + C \sin k_L(s - x) & \ell_1 \leq x \leq s \quad (1.52b) \\ D \sin k_L(q + x) + E \sin k_L(s - x) & -\ell_3 \leq x \leq 0 \quad (1.52c) \\ D \sin k_L(q + x) + F \sin k_L(q + x) & -q \leq x \leq -\ell_3 \quad (1.52d) \end{cases}$$

where

$$A = \frac{j2V_0}{Z_c} \frac{\sin k_L q}{\sin k_L(s + q)} - \frac{j2V_2}{Z_c} \frac{\sin k_L \ell_4}{\sin k_L(s + q)} \quad (1.53a)$$

$$B = -\frac{j2V_1}{Z_c} \frac{\sin k_L \ell_2}{\sin k_L(s + q)} \quad (1.53b)$$

$$C = -\frac{j2V_1}{Z_c} \frac{\sin k_L(q + \ell_1)}{\sin k_L(s + q)} \quad (1.53c)$$

$$D = j \frac{2(V_0 \sin k_L s - V_1 \sin k_L \ell_2)}{Z_c \sin k_L(s + q)} \quad (1.53d)$$

$$E = -\frac{j2V_2}{Z_c} \frac{\sin k_L \ell_4}{\sin k_L(q + s)} \quad (1.53e)$$

$$F = -\frac{j2V_2}{Z_c} \frac{\sin k_L(s + \ell_3)}{\sin k_L(q + s)} \quad (1.53f)$$

and

$$V_1 = \{jZ_1V_0^e \sin k_L\ell_2[Z_c \sin k_Lq \sin k_L(s + q) + jZ_2 \sin k_Lq \sin k_L\ell_4 \times \sin k_L(s + \ell_3) - jZ_2 \sin k_Ls \sin^2 k_L\ell_4]\}/\text{Denom.} \quad (1.53g)$$

$$V_2 = \{jZ_2V_0^e \sin k_L\ell_4[Z_c \sin k_Ls \sin k_L(s + q) + jZ_1 \sin k_Ls \sin k_L\ell_2 \times \sin k_L(q + \ell_1) - jZ_1 \sin k_Lq \sin^2 k_L\ell_2]\}/\text{Denom.} \quad (1.53h)$$

with

$$\text{Denom.} = Z_c^2 \sin^2 k_L(s + q) + jZ_2Z_c \sin k_L(s + q) \sin k_L\ell_4 \sin k_L(s + \ell_3) + jZ_1Z_c \sin k_L\ell_2 \sin k_L(q + \ell_1) \sin k_L(s + q) - Z_2Z_1 \sin k_L\ell_2 \times \sin k_L\ell_4 \sin k_L(s + \ell_3) \sin k_L(q + \ell_1) + Z_1Z_2 \sin^2 k_L\ell_2 \times \sin^2 k_L\ell_4 \quad (1.53i)$$

Since all the antennas that will be considered are actually special cases of the configuration in Fig. 1.9 of [2], the $\bar{A}$ factor will be evaluated in this most general case and reduction to more special cases will be left till later. Considering the section of antenna from $0 \leq x \leq s$, it is straightforward to show that substituting (1.52a,b) into (1.50) gives:

$$\bar{A}_+ = A\{\int_0^{\ell_1} \sin k_L(s - x')e^{j\beta_0 \cos\phi \sin\theta x'} dx' + \int_{\ell_1}^{s} \sin k_L(s - x') \times e^{j\beta_0 \cos\phi \sin\theta x'} dx'\} + B\int_0^{\ell_1} \sin k_L(q + x')e^{j\beta_0 \cos\phi \sin\theta x'} dx' + C\int_{\ell_1}^{s} \sin k_L(s - x')e^{j\beta_0 \cos\phi \sin\theta x'} dx' \quad (1.54)$$

The solution for (1.54) is quite simple and necessitates the evaluation of

the following two types of integrals:

$$I_1 = \int_a^b \sin k_L(s - x) e^{j\beta_0 \cos\phi \sin\theta\, x}\, dx \tag{1.55}$$

$$I_2 = \int_a^b \sin k_L(q + x) e^{j\beta_0 \cos\phi \sin\theta\, x}\, dx \tag{1.56}$$

By making the following substitutions in I_1

$$s - x = \zeta \quad , \quad dx = -d\zeta \quad , \quad x = s - \zeta$$

one obtains

$$I_1 = -e^{j\beta_0 s \cos\phi \sin\theta} \int_{s-a}^{s-b} \sin(k_L\zeta) e^{-j\beta_0 \cos\phi \sin\theta\, \zeta}\, d\zeta \tag{1.57}$$

$$I_1 = \frac{1}{k_L^2 - \beta_0^2 \cos^2\phi \sin^2\theta} \{e^{j\beta_0 b \cos\phi \sin\theta} [j\beta_0 \cos\phi \sin\theta \times \sin k_L(s - b) + k_L \cos k_L(s - b)] - e^{j\beta_0 a \cos\phi \sin\theta} \times [j\beta_0 \cos\phi \sin\theta \sin k_L(s - a) + k_L \cos k_L(s - a)]\} \tag{1.58}$$

where (1.58) is obtained from an evaluation of the standard integral form in (1.57) [18]. Using a similar set of substitutions for I_2, namely,

$$q + x = \zeta' \quad , \quad d\zeta' = dx \quad , \quad x = \zeta' - q$$

the following can be ascertained:

$$I_2 = e^{-j\beta_0 q \cos\phi \sin\theta} \int_{q+a}^{q+b} \sin(k_L\zeta') e^{j\beta_0 \cos\phi \sin\theta\, \zeta'}\, d\zeta' \tag{1.59}$$

$$I_2 = \frac{1}{k_L^2 - \beta_0^2 \cos^2\phi \sin^2\theta} \{e^{j\beta_0 b \cos\phi \sin\theta} [j\beta_0 \cos\phi \sin\theta$$

[continued]

$$\times \sin k_L(q + b) - k_L \cos k_L(q + b)] - e^{j\beta_0 a \cos\phi \sin\theta}$$

$$\times [j\beta_0 \cos\phi \sin k_L(q + a) - k_L \cos k_L(q + a)]\} \qquad (1.60)$$

With the use of (1.58) and (1.60) the determination of $\bar{A}_+$ is straightforward and turns out to be:

$$\bar{A}_+ = \frac{A}{k_L^2 - \beta_0^2 \cos^2\phi \sin^2\theta} \{e^{j\beta_0 \ell_1 \cos\phi \sin\theta} [j\beta_0 \cos\phi \sin\theta \sin k_L \ell_2$$

$$+ k_L \cos k_L \ell_2] - [j\beta_0 \cos\phi \sin\theta \sin k_L s + k_L \cos k_L s]\}$$

$$+ \frac{B}{k_L^2 - \beta_0^2 \cos^2\phi \sin^2\theta} \{e^{j\beta_0 \ell_1 \cos\phi \sin\theta} [j\beta_0 \cos\phi \sin\theta \sin k_L(q + \ell_1)$$

$$- k_L \cos k_L(q + \ell_1)] - [j\beta_0 \cos\phi \sin\theta \sin k_L q - k_L \cos k_L q]\}$$

$$+ \frac{A}{k_L^2 - \beta_0^2 \cos^2\phi \sin^2\theta} \{k_L e^{j\beta_0 s \cos\phi \sin\theta} - e^{j\beta_0 \ell_1 \cos\phi \sin\theta}$$

$$\times [j\beta_0 \cos\phi \sin\theta \sin k_L \ell_2 + k_L \cos k_L \ell_2]\} + \frac{C}{k_L^2 - \beta_0^2 \cos^2\phi \sin^2\theta}$$

$$\times \{k_L e^{j\beta_0 s \cos\phi \sin\theta} - e^{j\beta_0 \ell_1 \cos\phi \sin\theta} [j\beta_0 \cos\phi \sin\theta \sin k_L \ell_2$$

$$+ k_L \cos k_L \ell_2]\} \qquad (1.61)$$

Similarly, for the section of antenna from $-q \leq x \leq 0$

$$\bar{A}_- = D\{\int_{-\ell_3}^{0} \sin k_L(q + x') e^{j\beta_0 \cos\phi \sin\theta x'} dx' + \int_{-q}^{-\ell_3} \sin k_L(q + x')$$

$$\times e^{j\beta_0 \cos\phi \sin\theta x'} dx'\} + E \int_{-\ell_3}^{0} \sin k_L(s - x') e^{j\beta_0 \cos\phi \sin\theta x'} dx'$$

[continued]

$$+ F \int_{-q}^{-\ell_3} \sin k_L(q + x')e^{j\beta_0 \cos\phi \sin\theta\, x'} dx' \qquad (1.62)$$

Evaluating the above integrals with the help of (1.60) and (1.58) leads to the following:

$$\bar{A}_- = \frac{D}{k_L^2 - \beta_0^2 \cos^2\phi \sin^2\theta} \{j\beta_0 \cos\phi \sin\theta \sin k_L q - k_L \cos k_L q$$

$$- e^{-j\beta_0 \ell_3 \cos\phi \sin\theta} [j\beta_0 \cos\phi \sin\theta \sin k_L \ell_4 - k_L \cos k_L \ell_4]\}$$

$$+ \frac{E}{k_L^2 - \beta_0^2 \cos^2\phi \sin^2\theta} \{j\beta_0 \cos\phi \sin\theta \sin k_L s + k_L \cos k_L s$$

$$- e^{-j\beta_0 \ell_3 \cos\phi \sin\theta} [j\beta_0 \cos\phi \sin\theta \sin k_L(s + \ell_3) + k_L \cos k_L(s + \ell_3)]\}$$

$$+ \frac{D}{k_L^2 - \beta_0^2 \cos^2\phi \sin^2\theta} \{e^{-j\beta_0 \ell_3 \cos\phi \sin\theta} [j\beta_0 \cos\phi \sin\theta \sin k_L \ell_4$$

$$- k_L \cos k_L \ell_4] + k_L e^{-j\beta_0 q \cos\phi \sin\theta}\} + \frac{F}{k_L^2 - \beta_0^2 \cos^2\phi \sin^2\theta}$$

$$\times \{e^{-j\beta_0 \ell_3 \cos\phi \sin\theta} [j\beta_0 \cos\phi \sin\theta \sin k_L \ell_4 - k_L \cos k_L \ell_4]$$

$$+ k_L e^{-j\beta_0 q \cos\phi \sin\theta}\} \qquad (1.63)$$

With this the total far-field factor $\bar{A}$ can be obtained from (1.61) and (1.63) as:

$$\bar{A} = \bar{A}_+ + \bar{A}_- \qquad (1.64)$$

Once the $\bar{A}$ factor has been evaluated, it is a simple matter to substitute (1.64) into (1.49) and (1.51) and to solve for the total surface- and space-wave fields. Due to the complexity of (1.64), particularly for the

case of asymmetric drive, further simplification will not be attempted. Since $\bar{A}$ represents the most general situation, any of the cases discussed in Part I of [2] can be considered by imposing the necessary restrictions on the parameters involved. Obviously for the case of a symmetric-drive voltage, $\bar{A}_+ = \bar{A}_-$. As a check on (1.64) the special case of a center-driven dipole antenna with $k_L = \beta_0$ will be investigated. For this situation the following conditions are imposed: $\ell_1 = \ell_3$, $\ell_2 = \ell_4$, $s = q$ and $Z_1 = Z_2 = 0$. With these conditions it is easy to show that:

$$A = D \quad , \quad B = E = C = F = 0$$

and

$$\bar{A} = \frac{2A}{\beta_0^2 - \beta_0^2 \cos^2 \phi \sin^2 \theta} \{\beta_0 e^{j\beta_0 s \cos \phi \sin \theta} + \beta_0 e^{-j\beta_0 s \cos \phi \sin \theta} - 2\beta_0 \cos \beta_0 s\} \tag{1.65}$$

$$\bar{A} = \frac{2A}{\beta_0(1 - \cos^2 \phi \sin^2 \theta)} [\cos(\beta_0 s \cos \phi \sin \theta) - \cos \beta_0 s] \tag{1.66}$$

As anticipated, (1.66) is equivalent to the far-field factor for a dipole antenna in free space with an assumed sinusoidal current distribution.

1.5. Useful Antenna Parameters

With expressions for the antenna input impedance and far-zone radiation patterns developed, it is possible to utilize these quantities to introduce a number of basic parameters commonly used to describe antennas.

Efficiency

The efficiency of an antenna is defined as the ratio of the power radiated by the antenna to the power supplied by the antenna. In general, wire antennas have an efficiency of close to 100%. The only loss mechanism involved would be due to the finite conductivity of the antenna itself. For unloaded wire antennas in the presence of an imperfectly conducting earth, the radiating efficiency is still close to 100% even for cases in which α_L is quite large. This is because the loss associated with α_L is due to

radiation and is not a heat loss caused by finite conductivity. In the loaded-wire cases, such as the Beverage antenna, the resistive part of the load represents a lumped dissipative loss which decreases the antenna efficiency. The radiation efficiency for the loaded-wire case is:

$$\% \text{ Efficiency} = \frac{P_{in} - P_D}{P_{in}} \times 100\% \tag{1.67}$$

where P_{in} is the real power supplied to the antenna and given by

$$P_{in} = |V_0|^2 G_0 \tag{1.68}$$

and P_D is the power dissipated in the load, namely,

$$P_D = |I_{R_L}|^2 R_L \tag{1.69}$$

In (1.68) V_0 is the driving-point voltage and G_0 the input conductance of the antenna; in (1.69) I_{R_L} is the amplitude of the current at the load and R_L is the real part of the load impedance. For the Beverage antenna, $R_L = Z_c/2$. For loaded antennas with asymmetric drive, it is necessary to evaluate P_D for each load in order to obtain a total dissipated power. Expressions for current and input impedance developed in Part I of [2] can be used to obtain efficiencies for any of the cases previously investigated. Altschuler [19] has shown that for a traveling-wave antenna in free space the radiating efficiency is about 50%. For an identical configuration in the presence of an imperfect earth a higher efficiency would be expected. Efficiencies can be improved by loading the wire with a section of antenna, the input impedance of which is approximately equal to the matched load.

Front-to-Back Ratio

The front-to-back ratio is an important quantity specifically in dealing with the surface-wave radiation of the Beverage antenna. It is defined as the ratio of the peak power of the front lobe to the peak power of the back lobe where the front lobe is the main radiation lobe ($\phi = 0$) and the back lobe is a minor radiation lobe ($\phi = 180°$). Large front-to-back ratios are desirable and are a measure of the directivity of the antenna. For the surface wave with $\phi = 0°$ and $\theta = 90°$, the vertically polarized component

predominates at distances far from the source. From (1.51) it is evident that the directional properties for the z component are contained in the expression $\bar{A}\cos\phi$. Therefore, the front-to-back ratio in dB for the Beverage surface-wave field is:

$$\text{FBR} = 20\log_{10}\frac{\bar{A}_{BEV}(\theta = 90°,\ \phi = 0°)}{\bar{A}_{BEV}(\theta = 90°,\ \phi = 180°)} \tag{1.70}$$

where $\bar{A}_{BEV}$ is simply (1.64) subject to the asymmetrically driven Beverage conditions, i.e., $R_1 = R_2 = R_c$, $\ell_3 = 0$, $\ell_2 = \ell_4 = \lambda_L/4$. Experimentation has shown that with this configuration front-to-back ratios of 20 dB are easily obtainable.

Antenna Gain

The gain of an antenna is probably the most commonly used parameter for describing its directional radiation properties. The gain of an antenna in a specific direction is defined as 4π times the ratio of the radiation intensity in that direction to the total power P. The radiation intensity in a given direction is defined as the power per unit solid angle in that direction. When P is the total power supplied to the antenna, the gain is called the power gain. When P represents the total power radiated by the antenna, the gain is called the directive gain. For the space wave the power gain can be written as:

$$G_P(\theta,\phi) = \frac{4\pi R_0^2|E \times H^*|}{P_{in}} = \frac{R_0^2(|E_\theta|^2 + |E_\phi|^2)}{30P_{in}} \tag{1.71}$$

where P_{in} is given by (1.68). It is straightforward to show that the directive gain is:

$$G_D(\theta,\phi) = \frac{R_0^2(|E_\theta|^2 + |E_\phi|^2)}{30P_{rad}} \tag{1.72}$$

where $P_{rad} = P_{in} - P_D$. In (1.72) it has been assumed that the antenna is perfectly conducting and that P_D is the power dissipated in the resistive loads. Obviously for an efficient antenna, $G_D = G_P$. With (1.49) and the current expressions in (1.52), G_P and G_D can be evaluated readily from (1.71)

and (1.72). G_D and G_P can be evaluated for the surface wave by substituting $|E_z|^2$ for $(|E_\theta|^2 + |E_\phi|^2)$ in (1.71) and (1.72).

Effective Length

Until now most of the discussions have been concerned with parameters commonly used to describe antennas employed in a transmitting mode. The effective length of an antenna is a parameter used to indicate the effectiveness of the antenna as a transmitter or receiver of electromagnetic radiation. In actual use the effective length is more often referred to in analyzing the receiving properties of an antenna.

Under transmitting conditions the radiated field of an antenna in free space can be expressed in the form

$$\vec{E}_{trans} = j30\beta_0 \vec{h} I_0 \frac{e^{-j\beta_0 R_0}}{R_0} \tag{1.73}$$

where I_0 is the driving-point current and $\vec{h}$ is the complex effective length [20] with complex components h_θ and h_ϕ. From reciprocity considerations it can be shown that for an incident field with complex components $E_{0\theta}$ and $E_{0\phi}$ the open-circuit voltage induced on the receiving antenna is given by

$$V_{o.c.} = h_\theta E_{0\theta} + h_\phi E_{0\phi} = \vec{h} \cdot \vec{E}_0 \tag{1.74}$$

With (1.49) and (1.51) expressed in the form given by (1.73), the effective lengths for the space wave and surface wave of an antenna over an imperfect earth are:

Space Wave:

$$h_\theta = (\bar{A}/I_0)[e^{j\beta_0 d \cos\theta} \sin\phi\,(1 + R_h e^{-j2\beta_0 d \cos\theta})] \tag{1.75a}$$

$$h_\phi = -(\bar{A}/I_0)[e^{j\beta_0 d \cos\theta} \cos\phi \cos\theta\,(1 - R_v e^{-j2\beta_0 d \cos\theta})] \tag{1.75b}$$

Surface Wave:

$$h_\psi = (\bar{A}/I_0)\{e^{j\beta_0 d \cos\theta} \cos\phi\,[u(1 - u^2\cos^2\psi)^{1/2}](1 - R_v)$$

[continued]

$$\times F \cos\psi \left(1 + \frac{\sin^2\psi}{2}\right)\} \tag{1.76a}$$

$$h_\rho = (\bar{A}/I_0)e^{j\beta_0 d\cos\theta} \cos\phi \left[u^2(1 - u^2\cos^2\psi)(1 - R_v)F\right]$$

$$\times \left(\frac{1 - \sin^4\psi - \dfrac{(1 - R_h)G}{(1 - R_v)u^2F}}{1 - u^2\cos^2\psi} \right) \tag{1.76b}$$

$$h_\phi = (\bar{A}/I_0)e^{j\beta_0 d\cos\theta} \sin\phi\,(1 - R_h)G \tag{1.76c}$$

where the expressions for $\bar{A}$ and I_0 have been previously developed.

1.6. The Field of an Antenna in the Presence of a Conducting Half-Space: Recent Advances

The development previously presented is based on the work of Norton which was done nearly forty years ago and provides a good engineering approximation for the far-field of a dipole above an imperfect earth. Since then, however, more exact formulations have been developed that are worth mentioning. Probably the most extensive work dealing with this problem is contained in the monograph by Baños [21]. He deals specifically with the fields of vertical and horizontal dipoles in the presence of an imperfectly conducting half-space. His approach is entirely analytic and through the use of modified saddle-point techniques he has been able to evaluate the Sommerfeld integrals over a variety of asymptotic ranges. In addition to the far-field expressions, Baños was able to obtain analytic expressions in the near field and intermediate field ranges, though gaps exist between the various ranges of validity. Expressions were also obtained over various ranges for the fields in the imperfect conductor. Although no attempt was made to find field expressions for antennas of finite length, one could presumably superimpose Baños' results with a proper knowledge of the antenna current to obtain accurate expressions. Using the formulas for current obtained in Part I of [2] along with the development by King [22], accurate field calculations can be made for horizontal antennas and Beverage antennas over all ranges. This procedure was not included here since only the far-

field range was of immediate interest. It is important to note that in the more exact development by Baños the zeroth-order term in the far-field expressions is identical to that obtained by Norton.

With the advent of high-speed computers many numerical attempts have been made to evaluate the Sommerfeld integrals accurately [23], [24]. Due to the gaps that exist in the Baños formulation, numerical means were looked upon as a way to fill these gaps and also provide a check on Baños' work. The various approaches used are concerned with selecting the appropriate path of integration in the complex plane along which the Sommerfeld integrals can most easily be evaluated. The paths are judiciously chosen to reduce the effects of singularities in the integrand. These techniques are not always foolproof, and many times integration schemes are developed which work when dealing with one type of medium, but produce instabilities for another. Oftentimes different schemes are also necessary depending on whether the Sommerfeld integrals are being evaluated for near, intermediate or far-zone fields. With a knowledge of the correct current existing on the antenna, these numerical schemes can be utilized to provide adequate evaluation of the electromagnetic fields over all ranges of both media. These more exact numerical and analytic procedures show that the "geometric-optics" approximation for the far field of the horizontal dipole is good to within 10% of the approaches based upon the more accurate evaluation of the Sommerfeld integrals, [23].

PART II

EXPERIMENTAL MEASUREMENTS

2.1. Introduction

The current and charge distributions on an antenna are fundamental electrical quantities which can be used to determine all of the properties of the antenna. The developments in Part I have shown that with a knowledge of these distributions all radiation and transmission characteristics of the antenna can be obtained. Probably the most important characteristic is the antenna's radiation pattern, which describes how effectively an antenna directs radiated energy. Part II of this report is concerned with measurements made of the surface-wave radiation patterns of Beverage wave antennas placed over fresh water and dry earth. For the fresh water case, the measured field patterns are compared with theoretical results based on formulas (1.51) and (1.64). The current distributions used in (1.51) were obtained from the development in [2, Section 1.6, Eq. (1.52) with the values for k_L given by (1.7)]. Since this expression was shown to be not valid for earth at 300 MHz, the field-pattern measurements over dry earth are presented without theoretical comparisons.

The purpose of the measurements was essentially two-fold: first, to verify that the asymmetrically driven, modified Beverage antenna [2, Fig. 1.9] can be used to obtain unidirectional surface-wave and sky-wave radiation patterns equivalent to the radiation patterns of the conventional Beverage antenna; and secondly, to provide a check on the accuracy of the approximate formulation developed in Section 1.3, eq. (1.51). The measurements were made for a modified Beverage antenna, $1.0\lambda_0$ in length, placed at heights of $.01\lambda_0$, $.02\lambda_0$, $.05\lambda_0$, $.1\lambda_0$ and $.25\lambda_0$ above fresh water and dry earth. The measurements were mainly concerned with examining the vertical component of the surface wave since it can be shown [3] that in the radiation zone this represents the major field component for a horizontal radiating element in the presence of an imperfectly conducting half-space. All measurements were made on a scale model operating at the frequency 144.06 MHz. At this frequency the experiment represents a model scaled by a factor of five in relation to the full-scale situation operating at 30 MHz. At each height the load resistors were varied in an effort to obtain the largest front-to-back ratio and thus optimize the directivity of the surface-

wave radiation.

2.2. Experimental Equipment

In order to measure accurately the radiation patterns of Beverage antennas, special equipment had to be fabricated. Since radiation field pattern measurements must be made at a distance of many wavelengths from the source, with an operating frequency of 144.06 MHz the measurements had to be performed in a large open area such as a field or lake. The unavailability of electrical power in locations such as these made it necessary to have a transportable, battery-operated RF power source. Furthermore, for outdoor field-pattern measurements the conventional technique of driving the antenna against a ground plane could not be utilized for several reasons. First of all, it has been shown experimentally [25] that the presence of a finite-sized ground plane can significantly alter the radiation pattern from the idealized case where the ground plane is replaced by the image. Fields generated by currents and charges at the edge of the ground plane are the main cause of this problem. Only when ground planes are many wavelengths in size can this error be kept within acceptable limits. Secondly, the use of the ground plane precludes investigating the asymmetrically driven Beverage antenna which is the case of immediate interest due to its proposed radiation characteristics. Without the use of a ground plane, it was necessary to design a structure which could support the antenna at various heights above the water and earth. Furthermore, when the ground plane is absent, the need to transfer power from a coaxial feed line to an asymmetrically driven dipole will cause large unbalanced currents to exist on the outside of the coaxial line. To alleviate this problem, a balun was designed to maintain balanced currents on the feed line by preventing current from being generated on the outside of the coaxial line. These currents cause the coaxial transmission line to radiate, thus making the feed line part of the antenna system and producing a radiation pattern that can be quite different from that of the antenna alone. The balun is necessary to insure that field patterns being measured are due only to radiation from the modified Beverage antenna and are not being generated by some complicated combination of antenna and feeding system. In summary, to perform the field-pattern measurements it was necessary to fabricate a source of RF power which could be battery-operated, a supporting structure to hold the antenna which could be used over water

and earth, and a coaxial balun to suppress unbalanced currents on the antenna feed line.

An operating frequency of 144.06 MHz was chosen because numerous designs for battery-operated solid-state transmitters were available in this 2 meter band. Also, at this frequency the wavelength is small enough to make possible the implementation of antennas which are several wavelengths long. The transmitter was built from a schematic as shown in Fig. 2.1(a). The schematic represents a two meter FM transmitter commonly used in mobile ham equipment. It is all solid-state and is designed to run off a twelve-volt battery pack. An output power of two watts is obtainable into a 50 ohm load. Since the transmitter was used in CW operation, the modulator section found in the lower left-hand corner of Fig. 2.1(a) which consists of CR1 and the accompanying circuit elements was not included in the version built. The transmitter signal is generated initially by an 18 MHz crystal-controlled oscillator, Q1, which is tuned to the 4 harmonic to produce an output of 73 MHz. This signal is then sent through a doubler, Q2, to produce the output signal. From the doubler the signal passes through several stages of amplification to obtain the required output power level. For the transmitter that was built, an output of 1.8 watts into a 50 ohm load was obtained at an operating frequency of 144.06 MHz and at an efficiency of 48%. The transmitter was constructed on a printed circuit board and mounted in a 5" × 10" aluminum box as shown in the left half of Fig. 2.3(c). Holes were drilled in the box to provide sufficient ventilation and connectors were mounted on the outside of the box to provide terminals through which the battery could be applied and the RF output obtained.

To insure that a sufficient amount of RF power was available for all situations, it was decided to build a power amplifier which would boost the output power of the transmitter. The schematic for the amplifier which was built is shown in Fig. 2.1(b). The amplifier consists of one stage which, depending on the transistor used for Q1, can deliver up to 25 watts of power into a 50 ohm load. The amplifier was designed to provide an output of 12 watts with a nominal 2 watt input. In actual operation an output of 10 watts was obtained from the amplifier when supplied with 1.8 watts of input power from the transmitter. The amplifier was assembled and tested on a printed circuit board and then housed in a 5" × 7" aluminum box shown on the right in Fig. 2.3(c). In addition to providing an enclosure, the aluminum

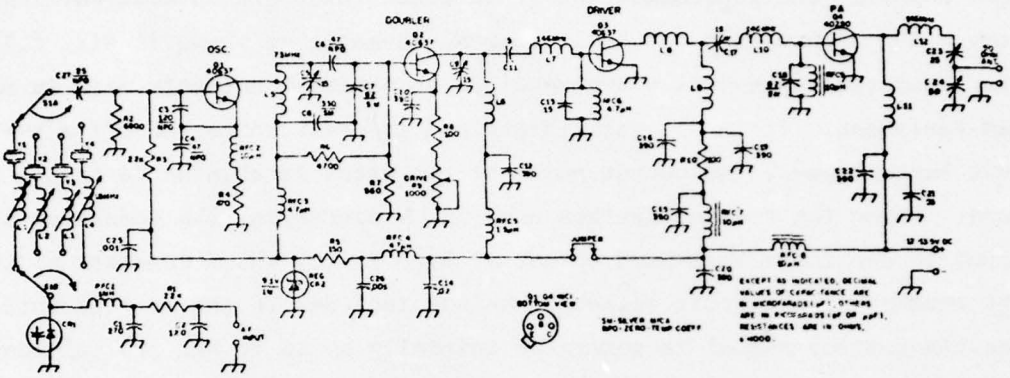

FIG. 2.1a. SCHEMATIC FOR RF TRANSMITTER

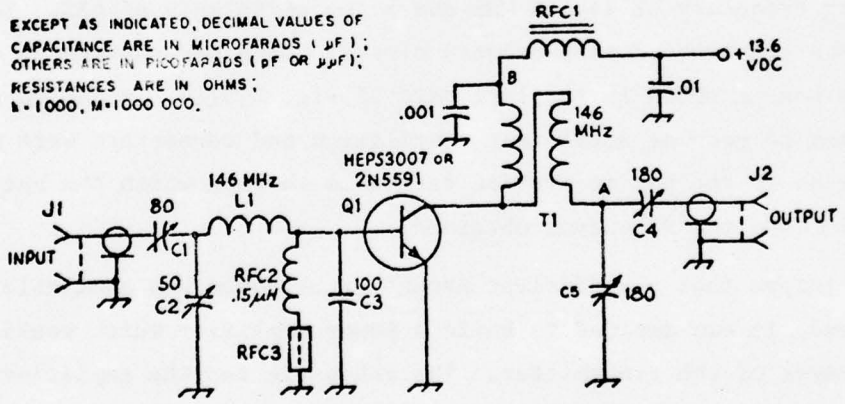

FIG. 2.1b. SCHEMATIC FOR 12W AMPLIFIER

box was used as a heat sink for Q1 which became extremely hot during operation.

The antenna itself was made of 1/8" brass tubing. To support the antenna over both water and earth, a polyfoam support was constructed as shown in Fig. 2.6(b). Polyfoam was used in the construction since it is a low-loss material with a dielectric constant very close to one, $\varepsilon_r \leq 1.1$, and will therefore have very little effect on the antenna and its field patterns. Polyfoam is also an excellent material to use for making floats - exactly what is needed to support the antenna over water. The combination float and support was constructed from two 1-3/4' × 8' polyfoam billets with a dielectric constant given as $\varepsilon_r = 1.03$. The two billets were placed 8" apart and seven polyfoam cross-members were glued between them. The polyfoam used for the cross-members was denser than the polyfoam from which the billets were constructed, yet the dielectric constant for the cross-member material was still quite low with a value of $\varepsilon_r = 1.07$. A series of holes was drilled in the cross-members so that the antenna could be placed at heights ranging from $.01\lambda_0$ to $.25\lambda_0$. The denser polyfoam made it easier to cut out uniform holes rather than having them torn out as would have been the case with the lighter polyfoam. The float was made as wide as possible to provide sufficient stability and thus prevent the possibility of having the float turn over in choppy water. When fully constructed, the float measured 4' × 8' with the center cross-members extending up to 2' in height. The total weight of the float was calculated to be approximately 52 pounds. Given this weight and the cross-sectional area of the float, it was determined that the float would sink approximately 8 mm into the water. This was determined to be a small enough perturbation so as to cause no real problem with the experimental model. To compensate for this two sets of holes were drilled, the second displaced from the first by 8 mm, one of which was used for the earth measurements and the other for water. The float proved to be a bit bulky but light enough to make transporting easy.

To prevent radiation from the antenna feed line, a balun was designed to operate at 144.06 MHz. The type of balun used was the standard bazooka or sleeve balun. The bazooka balun consists of a sleeve placed over a section of the coaxial feed line at the driving point. By short circuiting the sleeve to the outside of the coaxial feed line at a quarter wavelength back from the driving point, the sleeve and the outside conductor form a high

input impedance section of transmission line which suppresses any currents on the outside of the coaxial line. Suppression of these currents prevents the feed line from radiating. The balun has no effect on the impedance relationships between the antenna and the coaxial line. The construction of the balun and the feed line is depicted in Fig. 2.2. The feed line consists of RG 58 coaxial line with a characteristic impedance of 50 ohms. Where the coaxial line enters the sleeve section of the balun the outer rubber coating of the coaxial line was removed and the shield was soldered to the inside of a 1/4" O.D. piece of brass tubing. This forms the inner conductor for the transmission line consisting of the sleeve and the feed line. The sleeve was formed by a section of brass tubing of 7/8" O.D. and .033" wall thickness. The sleeve extended back from the driving point to a distance of 58 cm where it was short-circuited to the 1/4" tubing. At the driving point the shield and center conductor of the coaxial line were individually soldered to short sections of 1/8" brass tubing. The driving-point section was then encapsulated in a block of rexolite. This was done to provide a base and support to which longer lengths of 1/8" brass tubing could be attached to form the antenna. This was accomplished by screwing longer sections into the small pieces of tubing encased in the rexolite. Inside the sleeve section a sliding short circuit was constructed which could be used to tune out the unbalanced currents on the feed line. The short circuit consisted of a thin brass ring with copper beryllium fingers soldered to the inner and outer diameters of the ring. These fingers make continuous contact with the sleeve and inner conductor of the balun. Push rods were attached to the ring and the rods were extended beyond the sleeve section to provide external control for the positioning of the short circuit. An overall view of the balun and a close-up of the driving point are given in Figs. 2.3(a) and 2.3(b).

Once the balun was constructed it was necessary to calibrate it to insure its proper operation. This was accomplished by using the balun to feed a half-wave dipole antenna and then adjusting the short circuit to obtain the best balance on the feed line. This was checked initially by using a hand probe to sense the current on each element of the dipole. For a balanced feeding system the currents will be equal on the two elements. This technique was used only to get a rough estimate of where the short circuit should be positioned to achieve the best balance. A more accurate procedure

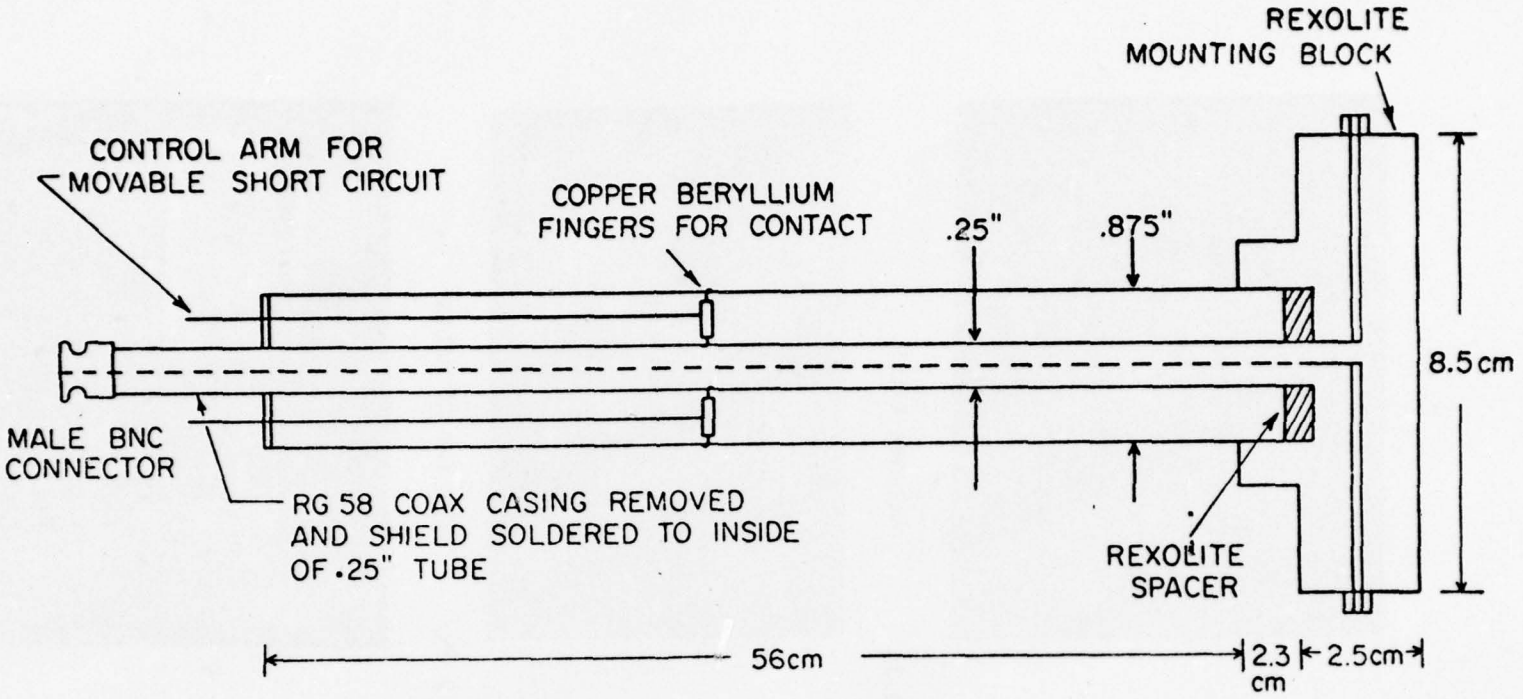

FIG. 2.2. BAZOOKA BALUN DESIGN FOR 144.06 MHz.

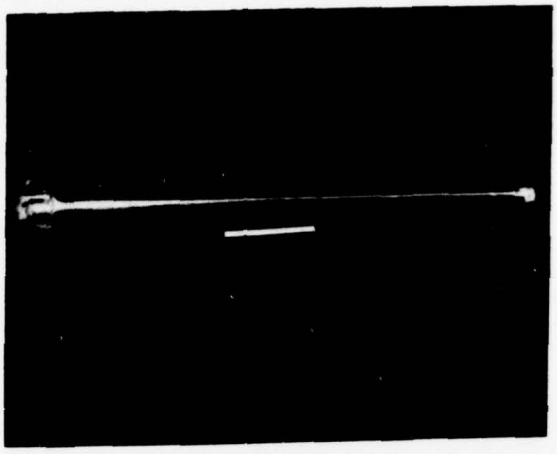

FIG. 2.3a BAZOOKA BALUN

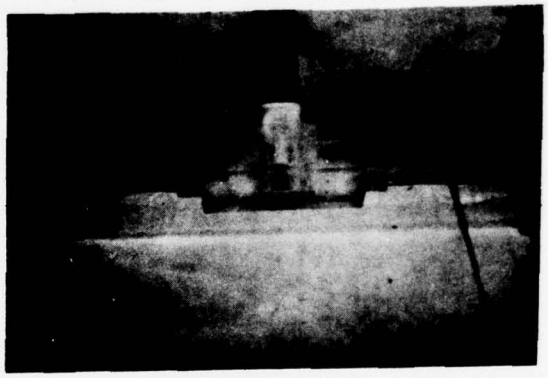

FIG. 2.3b FEED END OF BALUN

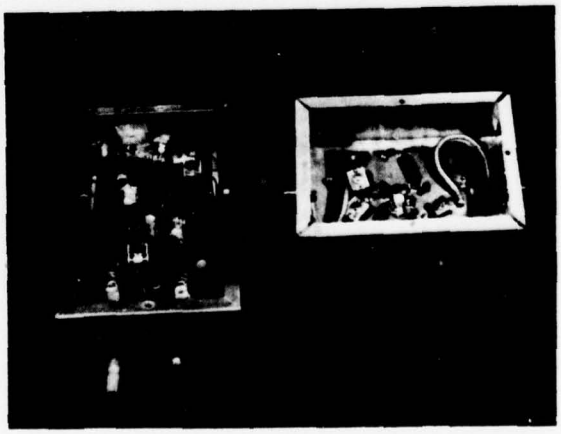

FIG. 2.3c SOLID-STATE TRANSMITTER AND AMPLIFIER

was then used in which the radiation pattern for the half-wave dipole was measured for various positions of the short circuit. It turns out that in many cases when an unbalanced condition exists on the antenna and feed line, asymmetry is observed in the antenna's radiation pattern, especially in the nulls. With this in mind, the short circuit was adjusted to obtain simultaneously as symmetrical a radiation pattern and as deep a null as possible. The condition on the depth of the null is necessary because radiation from the feed line may produce fields of greater intensity than the field produced at the null of the dipole radiation pattern. In this case the nulls will appear symmetric yet not as deep as they should be. By using these two criteria, the balun was adjusted until the optimum radiation pattern in Fig. 2.4 was obtained. For this pattern symmetric nulls of 33 dB were obtained. The pattern was measured at a distance of $25\lambda_0$, which easily falls within the radiation-zone condition. Once the proper setting on the short circuit was obtained, the push rods were permanently set in place with epoxy.

The field pattern in Fig. 2.4 and all subsequent field patterns were measured with the Rhode & Schwarz VHF field-strength meter shown in Fig. 2.8(b). The meter is actually a very sensitive heterodyne receiver which, when used with its accompanying half-wave dipole antenna, has a calibrated output that is proportional to the electric-field strength at the antenna. The meter can tune over the entire VHF band from 25 MHz to 300 MHz with a bandwidth of only 120 Kc. Field strengths as low as 1.5 μV/m can be detected with this meter. The meter can be used quite easily for outdoor field-pattern measurements since it is equipped to operate on rechargeable nickel-cadmium batteries. When used in conjunction with the accompanying dipole antenna, the meter was found to give accurate field-pattern measurements.

2.3. Beverage Antenna Field-Pattern Measurements: Techniques and Results

The measurement procedures used in both the fresh-water and dry-earth cases were quite similar except for special difficulties encountered with water due to mobility problems. The block diagram for the measurements is given in Fig. 2.5. The transmitter, amplifier, balun and field-strength meter have all been described in the previous section. A lead-acid car battery was used for the 12-volt power source. It was necessary to use a battery of this capacity because the transmitter and amplifier required over

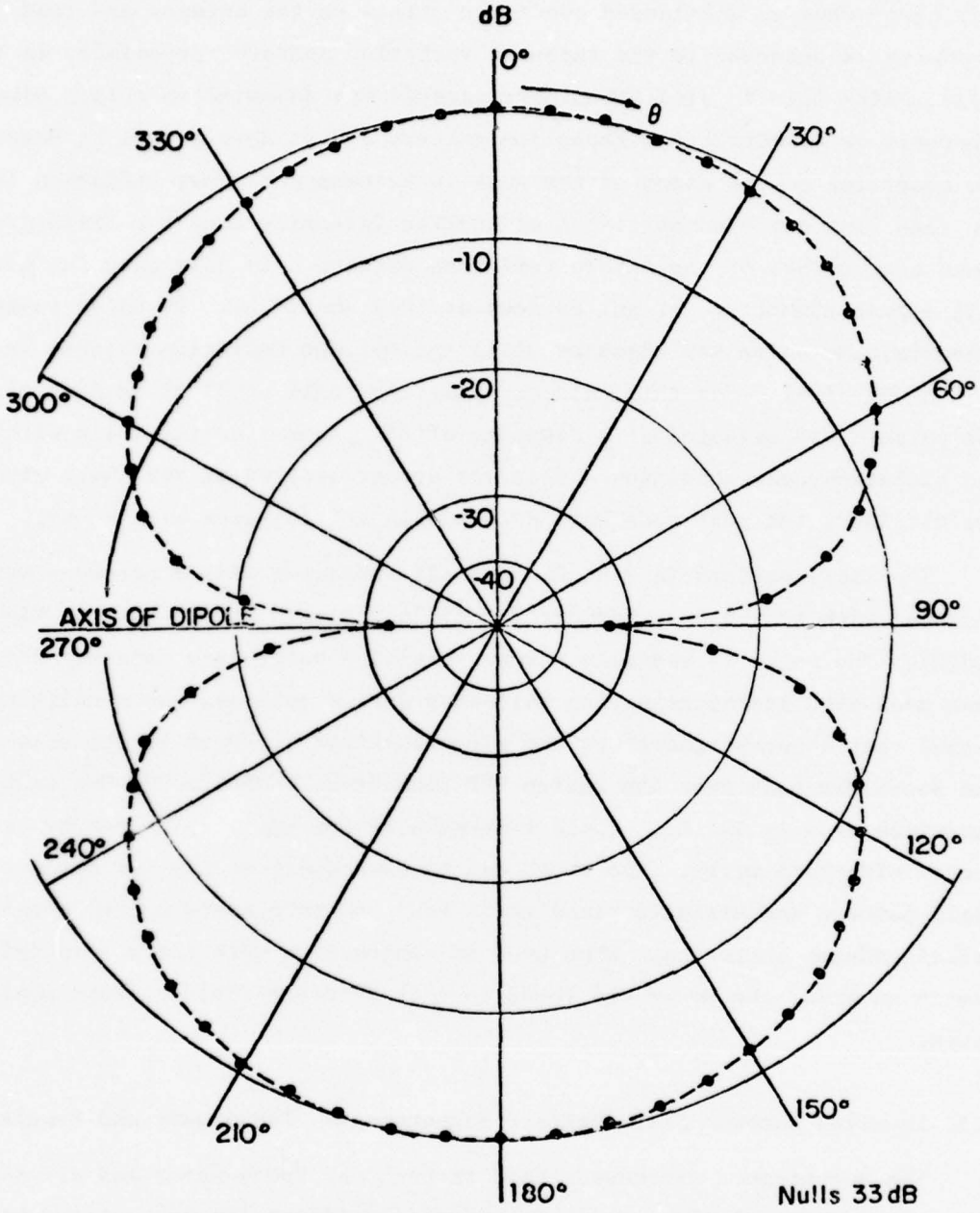

FIG. 2.4. SYMMETRIC VERTICAL RADIATION PATTERN OF QUARTER-WAVE DIPOLE DRIVEN WITH BAZOOKA BALUN.

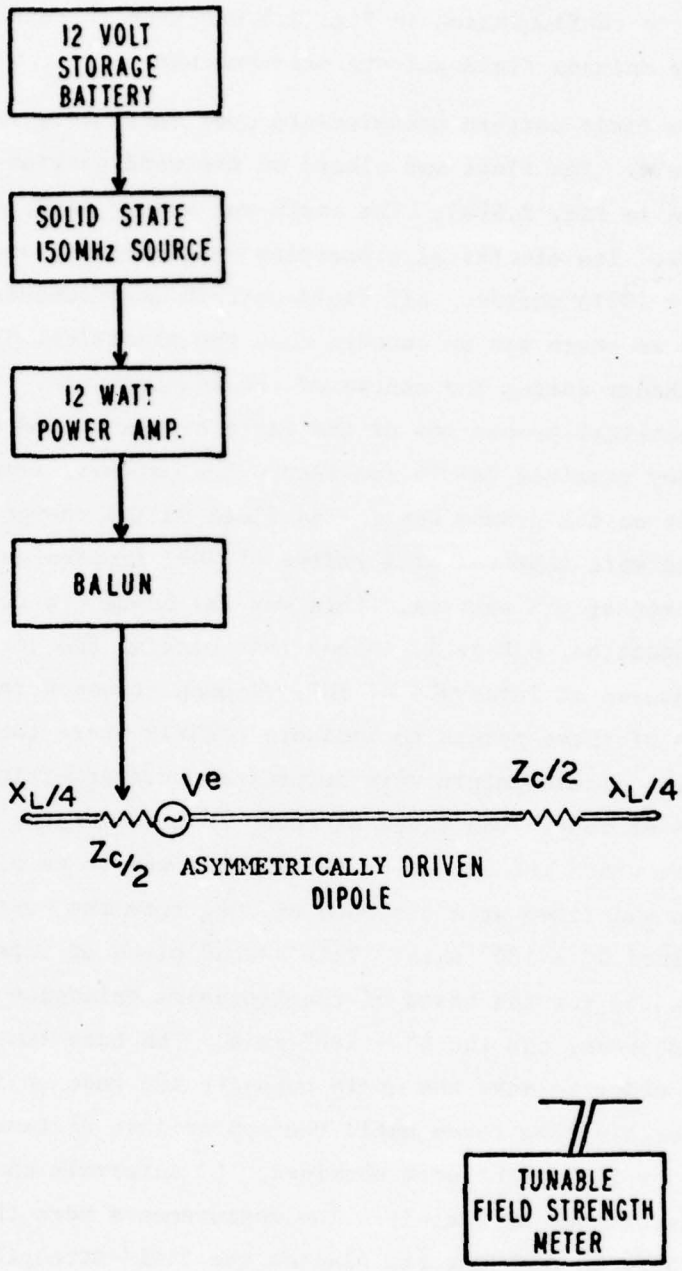

FIG. 2.5. BLOCK DIAGRAM FOR FIELD PATTERN MEASUREMENTS

1.5 Amps during operating times of several hours or more. The battery could then be recharged conventionally with an automobile battery charger. The asymmetric configuration in Fig. 2.5 was used throughout for all modified Beverage antenna field-pattern measurements.

The field-pattern measurements over earth were made on a large flat, open field. The float was placed on the sand portion of a baseball infield as shown in Fig. 2.6(a). The earth was a very hard, dry and granular-type material. Its electrical properties were measured and determined to be ε_r = 4.3, σ = .0013 mhos/m. All field-pattern measurements were to be made in one day so there was no concern that the electrical properties of the earth would change during the course of the measurements. Measurements made on the electrical properties of the earth over a period of several days showed that they remained fairly constant. The battery, transmitter and amplifier were set on the ground beside the float during operation. The surface-wave patterns were measured at a radius of $20\lambda_0$ (approximately 42 meters) from the center of the antenna. This was far enough to fulfill the radiation-zone condition, $\beta_0 R >> 1$. Along this circle, the vertical electric field was measured at intervals of 15°. Wooden stakes were placed in the ground at each of these points to indicate clearly where the measurements were to be taken. These points were determined trigonometrically by using two lengths of rope. One piece of rope, $20\lambda_0$ in length, was fastened at the point at which the center of the antenna was to be placed. A second piece of rope was fixed at a distance of $20\lambda_0$ from the center on an arbitrarily determined 0° - 180° axis. This second piece of rope had marked along it the lengths for the bases of the isosceles triangles formed by it, the first "radius" rope, and the 0° - 180° axis. The base lengths were properly chosen in order to make the angle opposite the base an integral multiple of 15°. By stretching the ropes until the appropriate distance from the center and the 0° or 180° point were obtained, 15° intervals on a circle of radius $20\lambda_0$ were determined accurately. The measurements were then made quite readily by walking to each marker, placing the field-strength meter over this point, as shown in Fig. 2.6(b), and recording the reading. To insure the accuracy, the calibration on the meter was rechecked before each reading.

A similar procedure was employed to measure the Beverage antenna field patterns over water, but with obviously many more problems arising. It was first necessary to find a convenient body of water over which the measure-

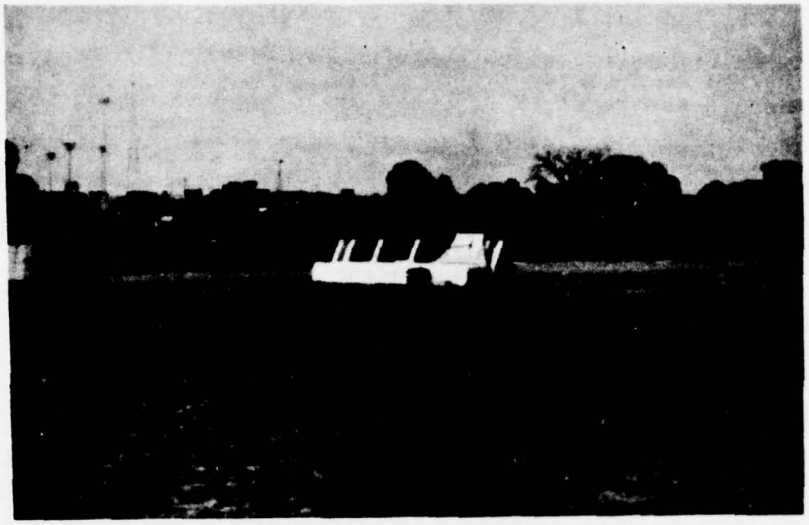

FIG. 2.6a ANTENNA FLOAT OVER DRY EARTH

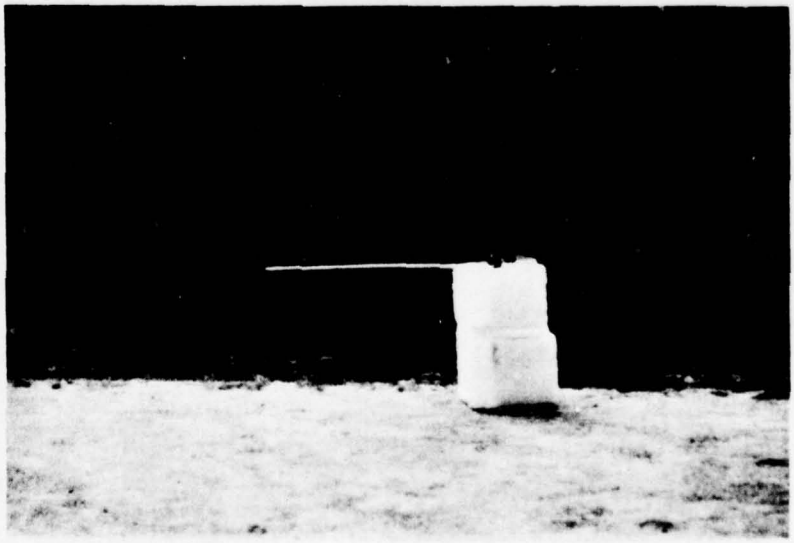

FIG. 2.6b FIELD-STRENGTH METER

ments could be made. Permission was granted by the M.D.C. to use a section of Upper Mystic Lake (Fig. 2.7a) to perform this research. One of the benefits of this particular lake was that no power boats were allowed to operate on it and thus create excessive turbulence. In order to maneuver on the lake, permission was received to use a small two-man rubber boat equipped with a 1-1/2 horsepower engine (Fig. 2.8b). A series of floats was placed in a semi-circle of radius $20\lambda_0$ at intervals of approximately 11°. This was accomplished by first establishing a center point by positioning a small float at approximately 230 feet from the shore. The water depth at this point was 45 feet and a large 100 pound weight was used to hold the float in place. A section of rope $20\lambda_0$ in length could then be tied on to the center float and pulled by the boat without moving the position of the center. Initially marker floats were dropped at 0° and 180° at a distance of $20\lambda_0$ from the center. The rest of the markers were placed by successively dividing the arc of the semi-circle in half, i.e., 90°, then 45°, etc. The division was mainly done visually. This resulted in errors of possibly as much as ±5° in each marker's location. With the use of the radius rope, however, it was fairly well assured that the floats all lay closely on a radius of $20\lambda_0$. Three additional floats, each anchored with 100 pounds of weight, were placed in a triangle around the center float. These were used to tie down the large float on which the antenna was placed (Fig. 2.7b). As can be seen in the figure, ropes were attached to the large float and were then tied securely to the trio of floats. When the antenna was in position, it was directed so that the main beam of radiation would be across the lake, resulting in no problems with reflections. The farthest measuring point from the shore, the 0° marker, was at a distance of 380 feet and the water depth was measured to be 66 feet. The closest measuring point to the shore, the 180° marker, was at a distance of 85 feet with a water depth of 10 feet. At all measuring points the water depth was greater than the skin depth, insuring that reflections off the bottom of the lake would not be a problem.

A separate smaller float was used to support the battery and transmitter as shown in Fig. 2.8(a). Holes were cut in the float into which the battery and electronics could be placed to avoid any movement in rough water. The equipment float was fastened securely to the larger float by means of ropes. The initial assemblage of floats and equipment was done on shore and then the entire apparatus was towed out by boat and tied down at the center.

FIG. 2.7a UPPER MYSTIC LAKE

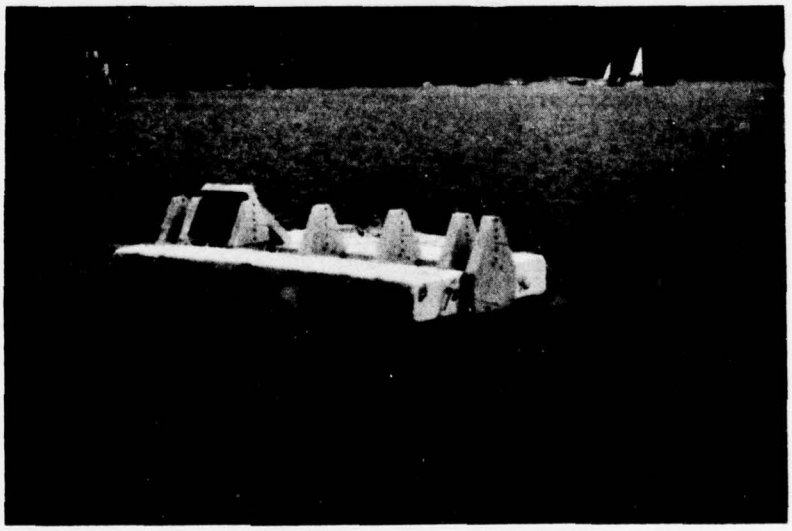

FIG. 2.7b ANTENNA FLOAT OVER FRESH WATER

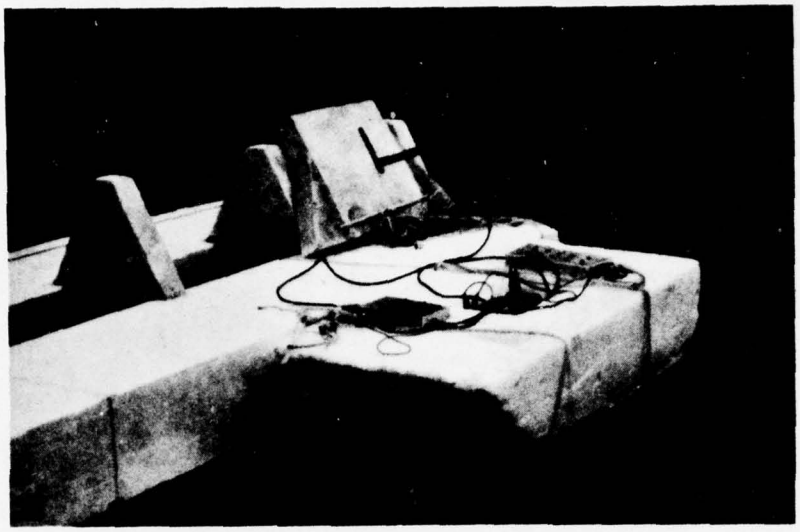

FIG. 2.8a EQUIPMENT FLOAT

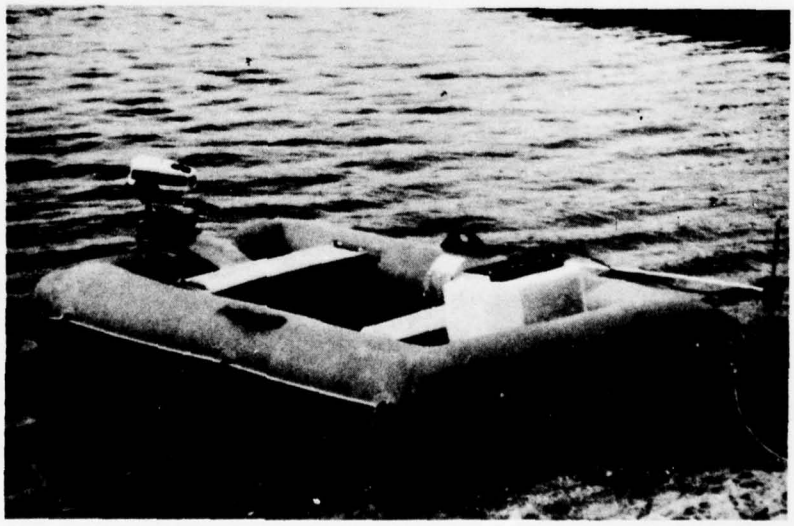

FIG. 2.8b RUBBER BOAT AND FIELD-STRENGTH METER

Once the floats were secured in the water, it was possible to change the antenna heights in this position from the boat without bringing the assembly back to shore. With the antenna height established, field-intensity measurements were made by moving the boat to each of the degree markers on the $20\lambda_0$ semi-circle and there recording the reading. To accomplish this two people were needed, one to navigate the boat and the other to take the readings. The meter was held in a block of polyfoam and positioned to the front of the boat in order that the antenna could extend beyond the bow, as shown in Fig. 2.8(b). Each measurement was made by moving radially in at the antenna and recording the reading as the boat passed over the marker float. Since any movement of the two persons in the boat could affect the readings, care was taken to remain as still as possible and to maintain the same relative positions for each set of measurements.

Over a period of time problems arose with marker floats disappearing due to vandals. With floats disappearing faster than they could be replaced, it was decided not to use all of the floats. Fortunately, the center float, the marker at 0° and the three anchored floats were all sufficiently weighted down so that they could not be moved. It was decided to retain only the 0°, 45°, 90°, 135° and 180° marker floats. At night these floats were tied about 1 foot under the water to prevent any further tampering. With fewer floats available, the measurement procedure was altered slightly. The boat was now made to move in a circular path using the 5 marker floats as guides and a watch was used to record measurements at intervals of 15 seconds. By assuming that the boat was moving at a constant rate, the 180° sweep could be divided by the number of readings to determine the angular position for each measurement. Obviously errors exist in the measurements due to uncertainties in the angular position and radial distance from the antenna but, considering the uncontrollable circumstances involved, every effort was made to minimize these errors.

Dry-Earth Measurements

As was previously mentioned, the field-pattern measurements were made over earth with electrical properties of $\varepsilon_r = 4.3$ and $\sigma = .0013$ mhos/m. To avoid any errors due to fluctuations in the transmitter's output power, a warm-up period of at least 15 minutes was observed before any measurements were taken. Bench testing has shown that good power output and frequency

stability can be obtained after 5 to 10 minutes of warm-up. A polyfoam canopy was placed over the transmitter and amplifier to shade them from the sun. Excessive heating of the aluminum boxes containing the electronics was discovered to cause transistor burn-outs and power drift. At each height a hand probe, consisting of a small loop, was used to determine approximately the phase constant β_L on the line. This was done by measuring the distance between nulls on the unloaded wire. From this the length of the quarter-wave sections can be determined. The resistor which gave the best front-to-back ratio was used for the pattern measurements.

The measured field patterns appear in Figs. 2.9 through 2.13. Tabulation of the measured data is given in Appendix A. The figures are presented in order of increasing d/λ_0; all are for an antenna of length $\ell_1 = \lambda_0$. In all cases except that in Fig. 2.9 only half of the surface-wave pattern, from 0° to 180°, was measured. In Fig. 2.9 the symmetry of the pattern was checked to determine if a possible unbalance in the feeding line or reflections from distant objects were affecting the pattern. Measurements made on a full 360° sweep show that the symmetry of the pattern is quite good with some small asymmetry appearing in the back lobe. The measurements presented are for the vertical component, E_z, which can be shown to be the major component of radiation in the surface wave. The horizontal surface-wave component, E_ϕ, was measured to be around 20 dB below the E_z component at all points except in the vicinity of 90° and 270° where the E_z pattern has a sharp null. At these two points E_z and E_ϕ are comparable in magnitude. The measurements in Figs. 2.9 through 2.12 show that with heights of $d/\lambda_0 = .01$ to .1 and with proper matching the modified Beverage antenna can achieve very directive radiation patterns with front-to-back ratios of close to 20 dB and half-power beamwidths of around 80°. These patterns are all quite similar, with some small variations appearing in the minor-lobe structure. At $d/\lambda_0 = .25$ (Fig. 2.13) the general shape of the pattern begins to change and the directivity suffers also. A dip in the major lobe at $\phi = 0°$ is observed and a front-to-back ratio of only 9 dB was obtained. It would appear that the departure of the current and charge distributions from a transmission-line form is manifested in this radiation pattern.

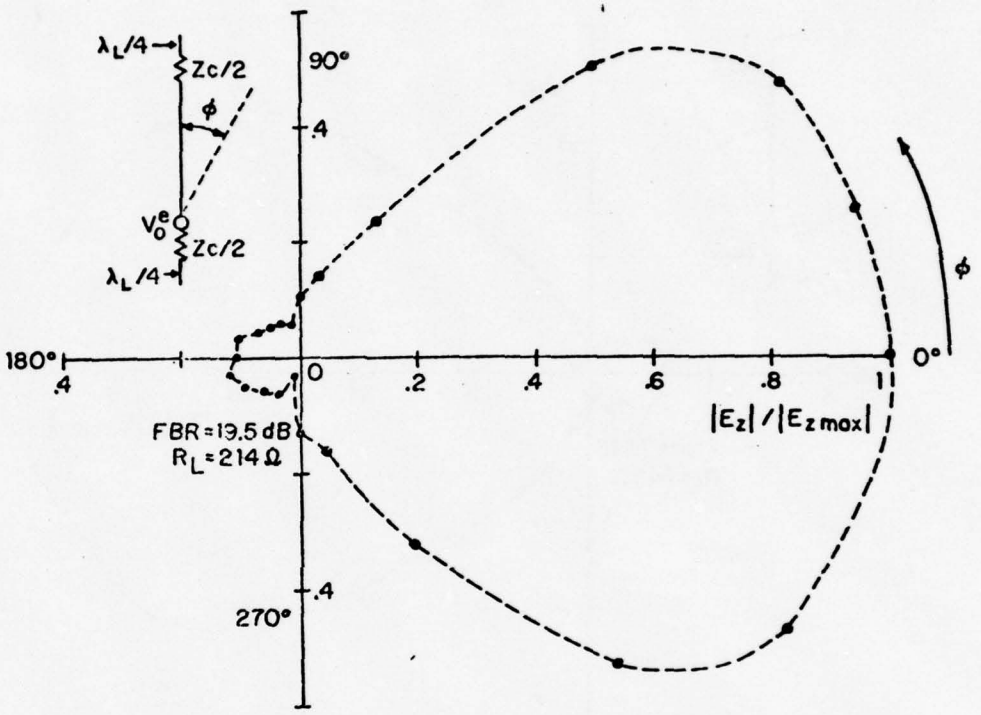

FIG. 2.9. MEASURED RELATIVE ELECTRIC FAR FIELD PATTERN FOR MODIFIED BEVERAGE ANTENNA OVER DRY EARTH. VERTICAL COMPONENT OF SURFACE WAVE WITH $d/\lambda_0 = .01$, $\ell_1/\lambda_0 = 1$, $\epsilon_r = 4.3$ AND $P_e = .038$.

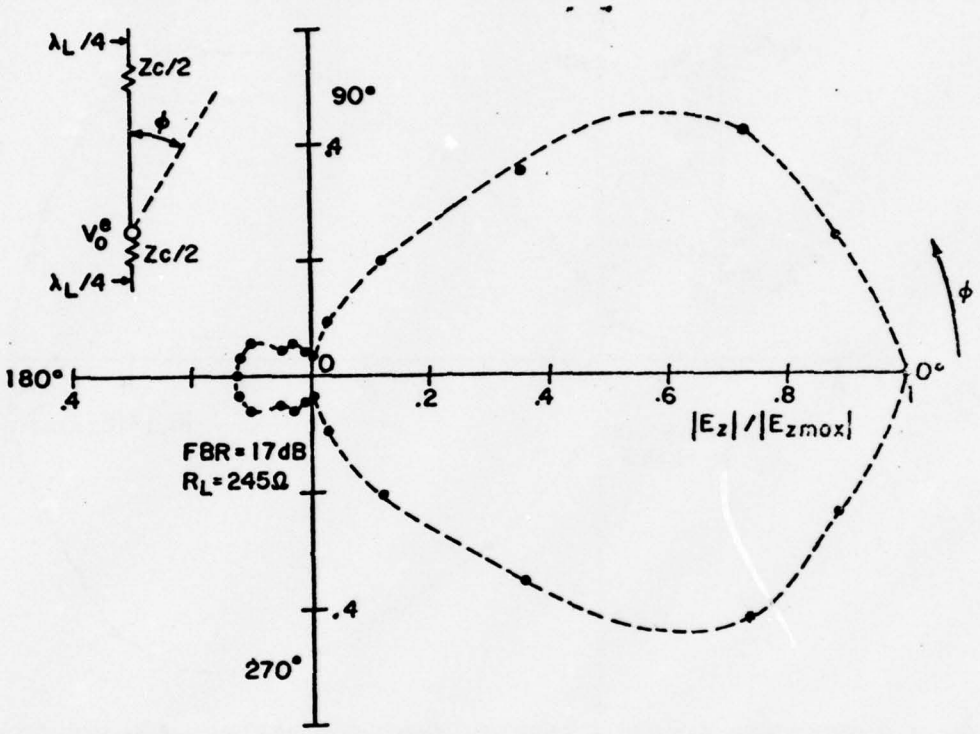

FIG. 2.10. MEASURED RELATIVE ELECTRIC FAR FIELD PATTERN FOR MODIFIED BEVERAGE ANTENNA OVER DRY EARTH. VERTICAL COMPONENT OF SURFACE WAVE WITH $d/\lambda_0 = .02$, $\ell_1/\lambda_0 = 1$, $\epsilon_r = 4.3$, AND $P_e = .038$.

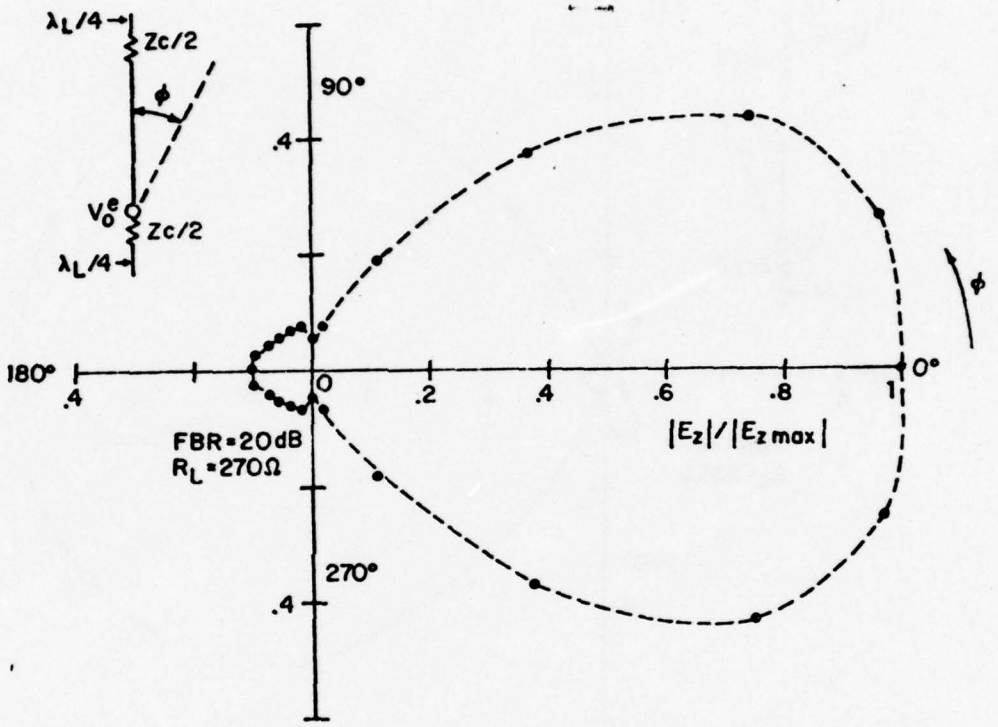

FIG. 2.11. MEASURED RELATIVE ELECTRIC FAR FIELD PATTERN FOR MODIFIED BEVERAGE ANTENNA OVER DRY EARTH. VERTICAL COMPONENT OF SURFACE WAVE WITH $d/\lambda_o = .05$, $\ell_1/\lambda_o = 1$, $\epsilon_r = 4.3$, AND $P_e = .038$.

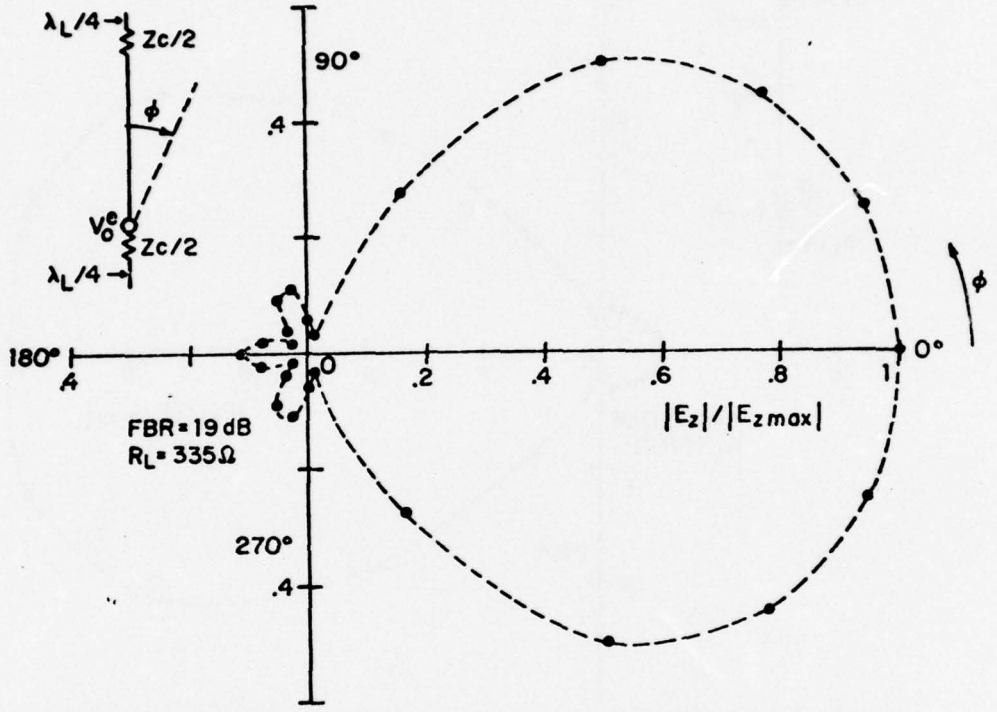

FIG. 2.12. MEASURED RELATIVE ELECTRIC FAR FIELD PATTERN FOR MODIFIED BEVERAGE ANTENNA OVER DRY EARTH. VERTICAL COMPONENT OF SURFACE WAVE WITH $d/\lambda_o = .1$, $\ell_1/\lambda_o = 1$, $\epsilon_r = 4.3$, AND $P_e = .038$.

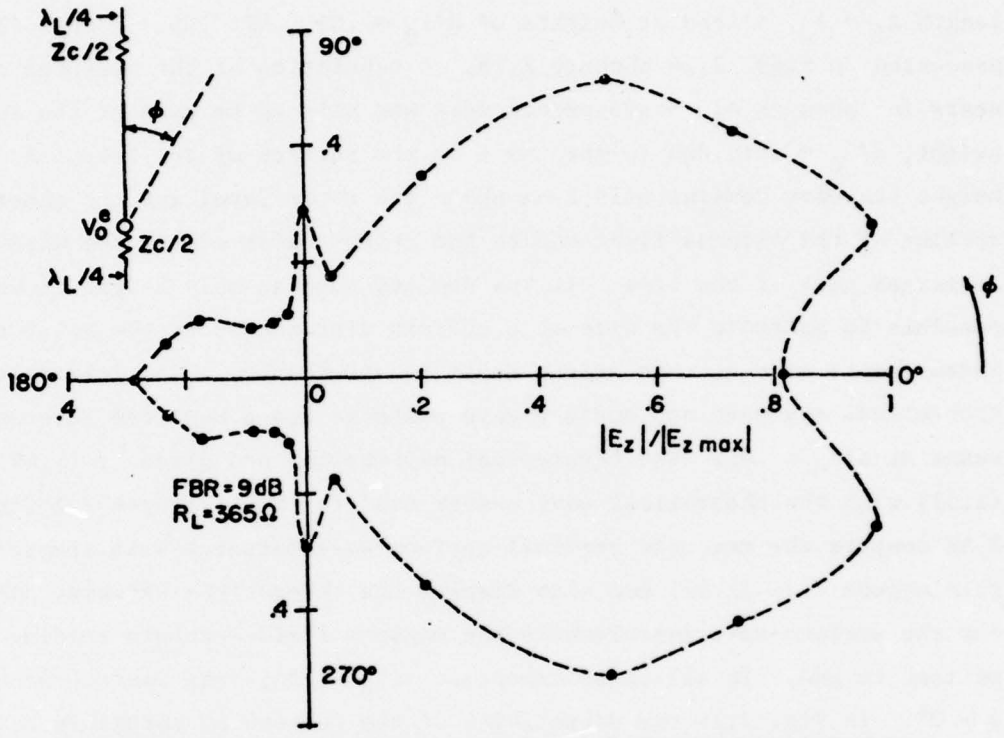

FIG. 2.13. MEASURED RELATIVE ELECTRIC FAR FIELD PATTERN FOR MODIFIED BEVERAGE ANTENNA OVER DRY EARTH. VERTICAL COMPONENT OF SURFACE WAVE WITH $d/\lambda_0 = .25$, $\ell_1/\lambda_0 = 1$, $\epsilon_r = 4.3$, AND $P_e = .038$.

Fresh-Water Measurements

Following a procedure similar to that used for the case over earth, measurements were made on modified Beverage antennas over fresh water. The water in Upper Mystic Lake was found to be highly conducting when compared to most fresh-water lakes. Its electrical properties were measured to be $\varepsilon_r = 81$ and $\sigma = .062$ mhos/m. In these measurements the values of $\lambda_L/4$ and $Z_c/2$ were determined from theoretical expressions given in [2, Eqs. (1.7) and (1.8)]. The measured field patterns for modified Beverage antennas of length $\ell_1 = \lambda_0$, placed at heights of $d/\lambda_0 = .01, .02, .05, .1$ and $.25$ are presented in Figs. 2.14 through 2.18. A tabulation of the measured data appears in Appendix A. Measurements were not able to be made at the lowest height, $d/\lambda_0 = .01$, due to the waves on the surface of the lake. At this height the wire remains only 2 cm above the water level and the constant rocking of the antenna float due to the choppy water caused the wire to be submerged part of the time. It was decided that at this height it was impossible to maintain the wire at a uniform distance above the water and that measurements made at this height would be unreliable. Fig. 2.14 shows the theoretical sky-wave and surface-wave patterns for a modified Beverage antenna at $d/\lambda_0 = .01$. The theoretical expressions are given by (1.49) and (1.51) with the theoretical wave number used for k_L. Figures 2.15 through 2.18 compare the measured vertical surface-wave patterns with theoretical predictions from (1.51) and also display the theoretical sky-wave patterns. For the surface-wave measurements the maximum field-strength reading is normalized to one. In all cases except at $d/\lambda_0 = .25$, this maximum occurs at $\phi = 0°$. In Fig. 2.15 the directivity of the pattern is certainly evident, but the field in the region $90° \leq \phi \leq 270°$ is much larger than the theory predicts. At this height the wire was still reasonably close to the water (approximately 4 cm) and the motion of the float could still cause large variations in the d/λ_0 value. Since this measurement was made over choppy water, it is reasonable to assume that this is the cause for the discrepancy in the back lobe. For the other three cases, Figs. 2.16 through 2.18, much better agreement is observed with slight variations appearing in the back lobe, which is quite sensitive to exact phase cancellations. It is interesting to note that at $d/\lambda_0 = .25$ a significant reduction in the front-to-back ratio is observed along with a dip in the main lobe at $\phi = 0°$ similar to the measurements over earth. The cause of this would again appear to

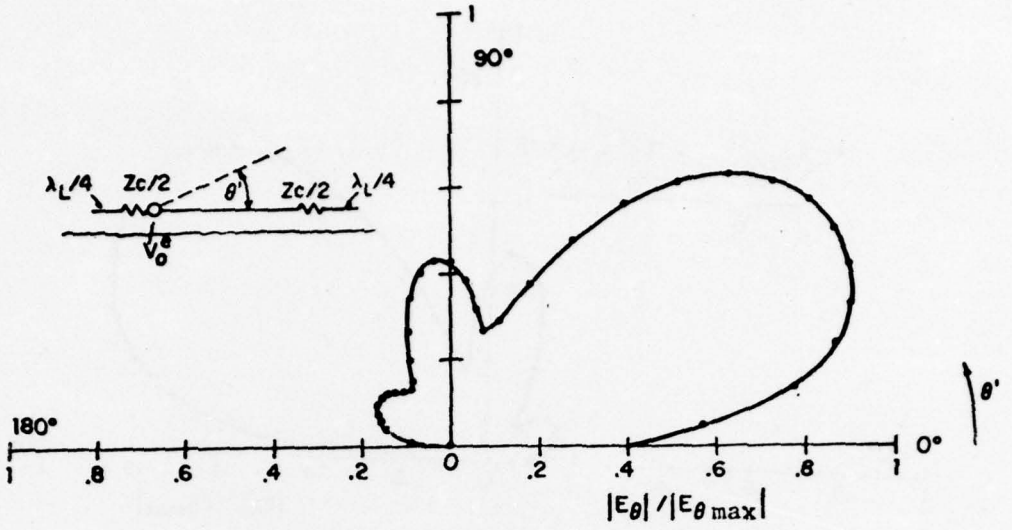

A) SKYWAVE FAR FIELD PATTERN

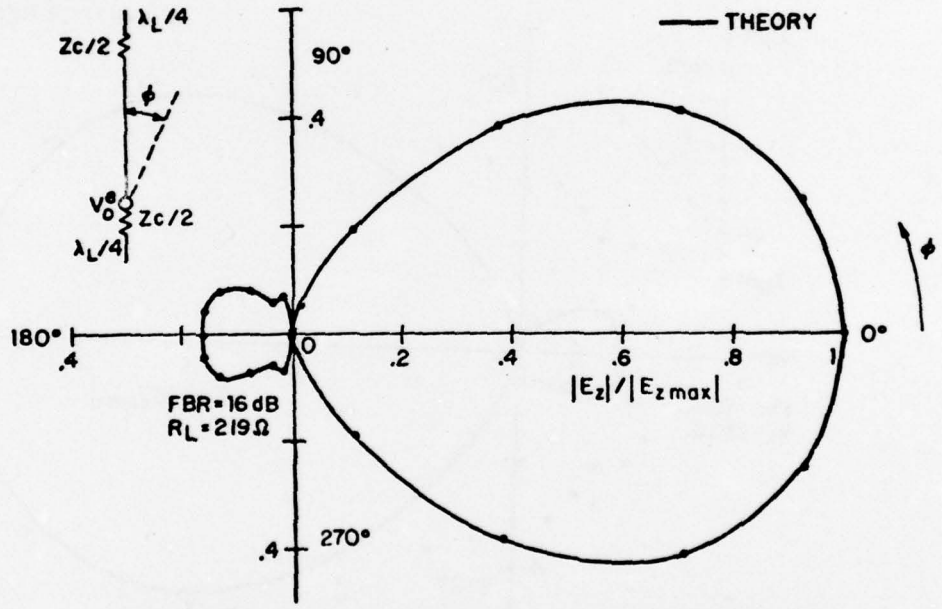

B) SURFACE WAVE FAR FIELD PATTERN; VERTICAL COMPONENT

FIG. 2.14. FAR FIELD PATTERNS FOR MODIFIED BEVERAGE ANTENNA OVER FRESH WATER; $d/\lambda_0 = .01$, $\ell_1/\lambda_0 = 1$, $\epsilon_r = 81$, AND $P_e = .097$

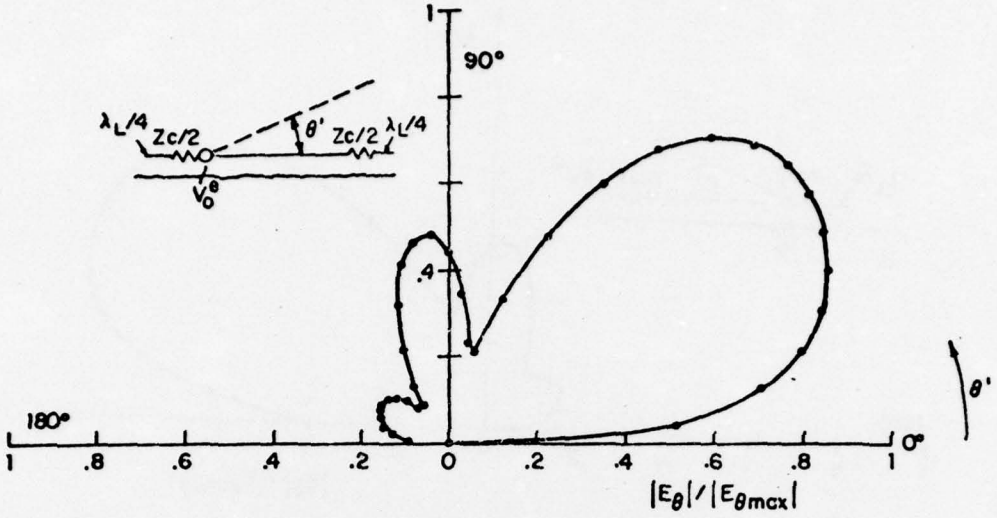

A) SKYWAVE FAR FIELD PATTERN

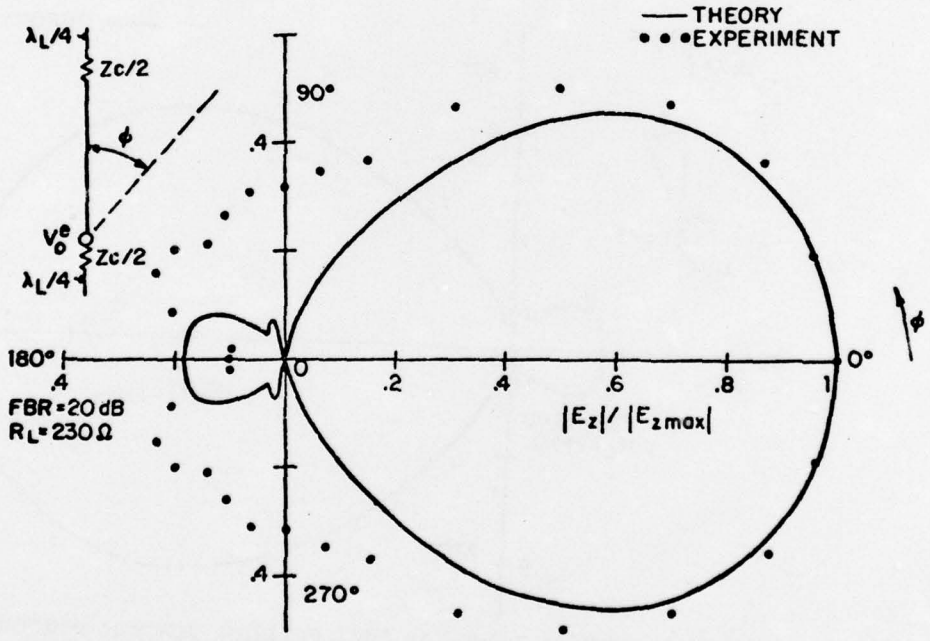

B) SURFACE WAVE FAR FIELD PATTERN; VERTICAL COMPONENT.

FIG. 2.15. FAR FIELD PATTERNS FOR MODIFIED BEVERAGE ANTENNA OVER FRESH WATER; $d/\lambda_0 = .02$, $\ell_1/\lambda_0 = 1$, $\epsilon_r = 81$, AND $P_e = .097$

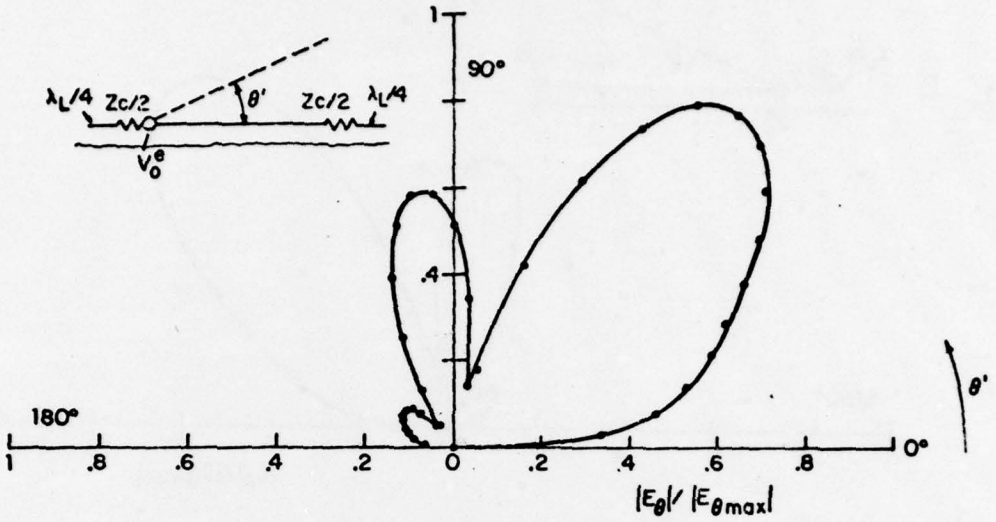

A) SKYWAVE FAR FIELD PATTERN

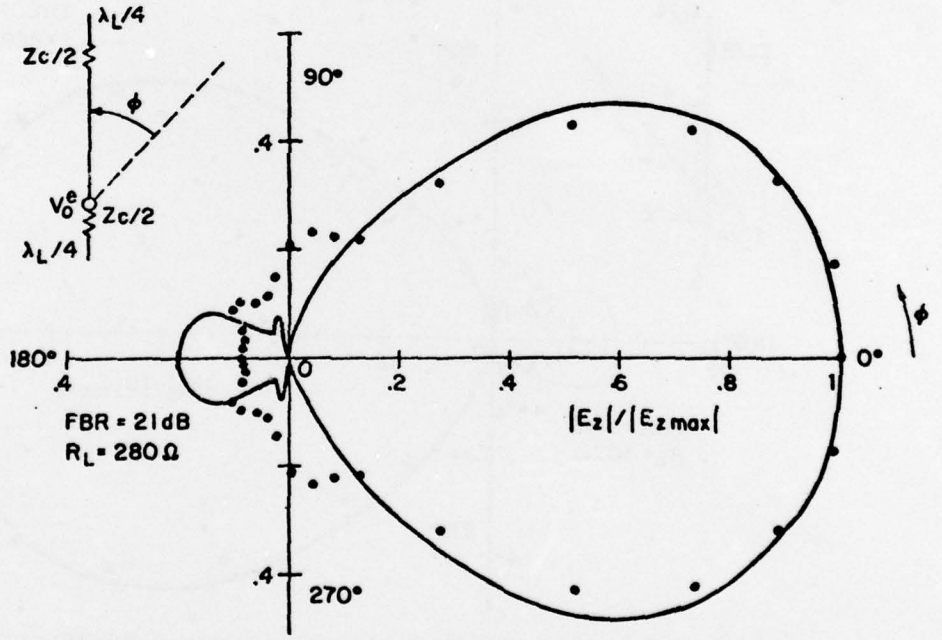

B) SURFACE WAVE FAR FIELD PATTERN; VERTICAL COMPONENT

FIG. 2.16. FAR FIELD PATTERNS FOR MODIFIED BEVERAGE ANTENNA OVER FRESH WATER; $d/\lambda_0 = .05$, $\ell_1/\lambda_0 = 1$, $\epsilon_r = 81$, AND $P_e = .097$.

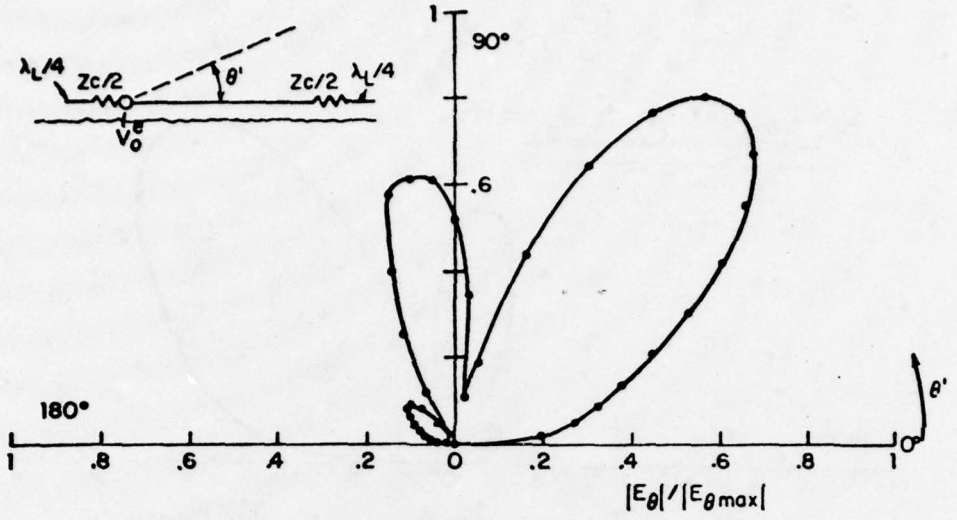

A) SKYWAVE FAR FIELD PATTERN

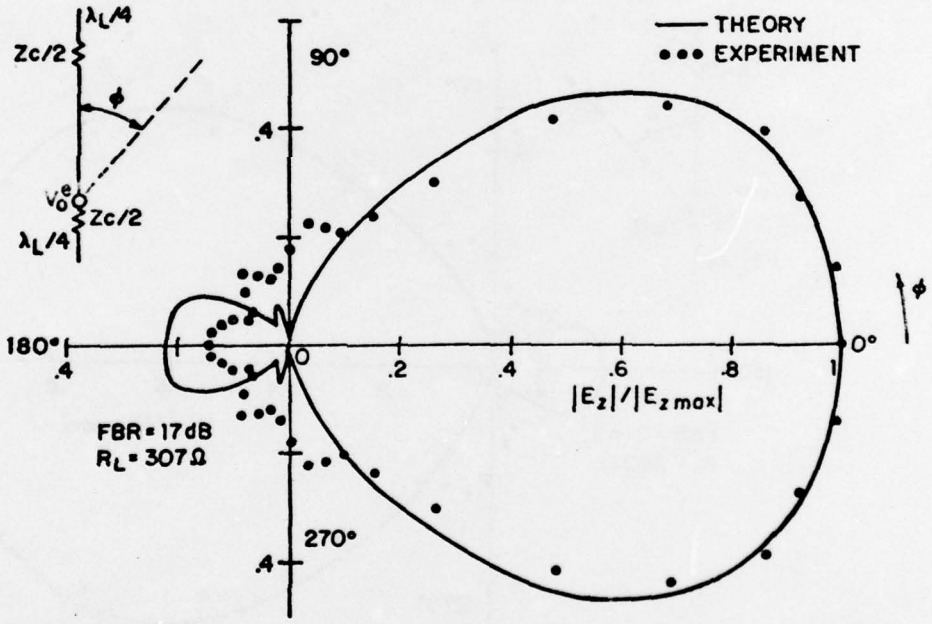

B) SURFACE WAVE FAR FIELD PATTERN; VERTICAL COMPONENT

FIG. 2.17. FAR FIELD PATTERNS FOR MODIFIED BEVERAGE ANTENNA OVER FRESH WATER; $d/\lambda_0 = .1$, $\ell_1/\lambda_0 = 1$, $\varepsilon_r = 81$, AND $P_e = .097$.

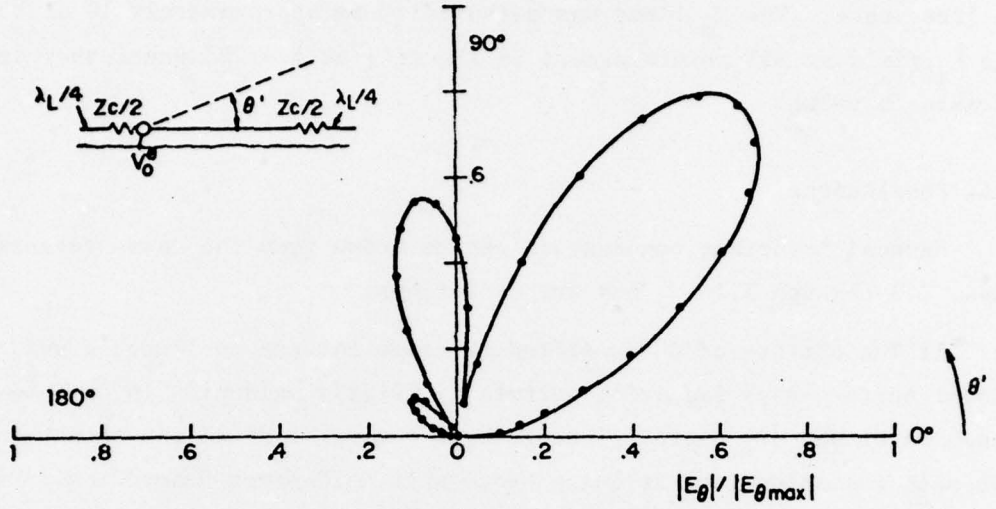

A) SKYWAVE FAR FIELD PATTERN

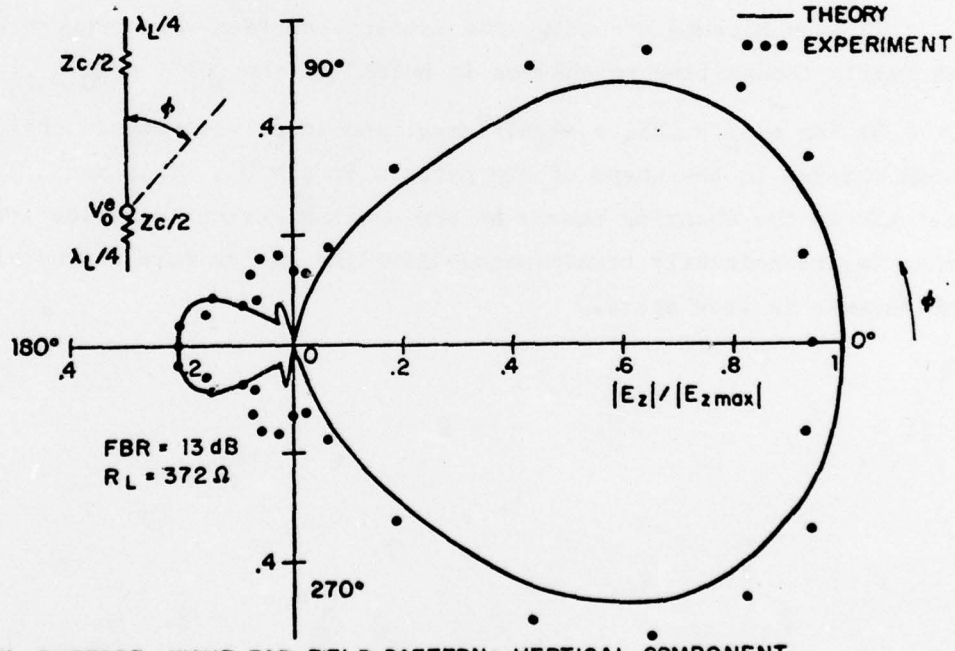

B) SURFACE WAVE FAR FIELD PATTERN; VERTICAL COMPONENT

FIG. 2.18. FAR FIELD PATTERNS FOR MODIFIED BEVERAGE ANTENNA OVER FRESH WATER; $d/\lambda_0 = .25$, $\ell_1/\lambda_0 = 1$, $\epsilon_r = 81$, AND $P_e = .097$.

be due to the changing nature of the current from one that is predominantly of transmission-line form to one that is more characteristic of an antenna in free space. The E_ϕ field was measured to be approximately 10 dB below the E_z field at all points except in the null at $\phi = 90°$ where they are comparable in value.

2.4. Conclusions

Several important conclusions can be drawn from the data presented in Figs. 2.9 through 2.18. They are as follows:

1) The ability of the modified Beverage antenna to launch a unidirectional surface-wave radiation pattern is clearly evident. In use over both fresh water and dry earth, front-to-back ratios of 20 dB can be obtained. The main radiation lobe is quite broad with half-power beamwidths of about 80°. Unidirectional characteristics should also be exhibited in the space-wave radiation pattern, although no measurements were made to confirm this. It would appear that the modified Beverage antenna should be an excellent element in highly directive broadside arrays.

2) When matched properly, the vertical surface-wave pattern appears to be fairly insensitive to changes in height in the $.01 \leq d/\lambda_0 \leq .1$ range.

3) For $d/\lambda_0 = .25$, a significant loss in directivity is noticed along with changes in the shape of the pattern at $\phi = 0°$. This seems to be attributable to the changing nature of the antenna current distribution from one that is predominantly transmission-line-like to one more characteristic of an antenna in free space.

APPENDIX A

TABLES OF THEORETICAL AND MEASURED FIELD PATTERNS OF BEVERAGE WAVE ANTENNAS

The tables in this appendix contain the theoretical and measured field patterns for modified Beverage antennas over fresh water. Also included are the measured data for Beverage antennas over dry earth. The following terms are defined:

"ETH/ETM" = E_θ normalized to the maximum E_θ value;

"EZ/EZM" = E_z normalized to the maximum E_z value;

"EFI/EZM" = E_ϕ normalized to the maximum E_z value;

"ERO/EZM" = E_ρ normalized to the maximum E_z value.

TABLE 2.1

FAR FIELD PATTERN OF BEVERAGE ANTENNA OVER FRESH WATER

D/LAMDAO = .0096 L1/LAMDAO = .560 RL = 219.08MMS

FREQUENCY = 144.1MHZ PE = .C97 ALFAL/BETAL = .1214 BETAL/BETAO = 1.117

E THETA SPACE(THEORY)

THETA	ETH/ETHM
.0	.000
5.0	.566
10.0	.783
15.0	.454
20.0	.958
25.0	.955
30.0	1.000
35.0	.986
40.0	.948
45.0	.884
50.0	.754
55.0	.679
60.0	.548
65.0	.411
70.0	.311
75.0	.280
80.0	.323
85.0	.384
90.0	.425
95.0	.421
100.0	.404
105.0	.349
110.0	.280
115.0	.213
120.0	.173
125.0	.158
130.0	.165
135.0	.179
140.0	.189
145.0	.192
150.0	.189
155.0	.181
160.0	.168
165.0	.151
170.0	.129
175.0	.091
180.0	.000

E FIELDS SURFACE(THEORY)

PHI	EZ/EZM	EFI/EZM	ERB/EZM
.0	1.00000	.00000	.10888
15.0	.96828	.00068	.10434
30.0	.81080	.00124	.08828
45.0	.53659	.00142	.05842
60.0	.21850	.00100	.02379
75.0	.04489	.00054	.00598
90.0	.00000	.00000	.00000
105.0	.04849	.00068	.00746
120.0	.06847	.00032	.00780
135.0	.10862	.00029	.01183
150.0	.15298	.00023	.01666
165.0	.16830	.00012	.01767
180.0	.16109	.00000	.01784
195.0	.16230	.00012	.01767
210.0	.15298	.00023	.01666
225.0	.10862	.00029	.01183
240.0	.06887	.00032	.00790
255.0	.06849	.00068	.00746
270.0	.00000	.00084	.00000
285.0	.05489	.00054	.00598
300.0	.21850	.00100	.02379
315.0	.53659	.00142	.05842
330.0	.81040	.00124	.08828
345.0	.95828	.00068	.10434
360.0	1.00000	.00000	.10888

FAR FIELD PATTERN OF BEVERAGE ANTENNA OVER FRESH WATER

D/LAMDAO = .0152 L1/LAMDAO = .960 RL = 230.08MMS

FREQUENCY = 144.1MHZ PE = .C97 ALFAL/BETAL = .0812 BETAL/BETAO = 1.045

E THETA SPACE(THEORY)

THETA	ETH/ETHM
.0	.000
5.0	.519
10.0	.712
15.0	.821
20.0	.895
25.0	.942
30.0	.977
35.0	.997
40.0	1.000
45.0	.977
50.0	.928
55.0	.829
60.0	.697
65.0	.533
70.0	.357
75.0	.223
80.0	.239
85.0	.347
90.0	.445
95.0	.485
100.0	.471
105.0	.422
110.0	.338
115.0	.243
120.0	.157
125.0	.108
130.0	.113
135.0	.140
140.0	.169
145.0	.179
150.0	.175
155.0	.175
160.0	.166
165.0	.153
170.0	.132
175.0	.094
180.0	.000

E FIELDS SURFACE(THEORY)

PHI	EZ/EZM	EFI/EZM	ERB/EZM
.0	1.00000	.00000	.10888
15.0	.96984	.00069	.10560
30.0	.84926	.00130	.09247
45.0	.59325	.00187	.06459
60.0	.25658	.00118	.02792
75.0	.03811	.00038	.00415
90.0	.00000	.00074	.00000
105.0	.07197	.00071	.00784
120.0	.05792	.00027	.00631
135.0	.08510	.00023	.00927
150.0	.15535	.00024	.01692
165.0	.18037	.00013	.01964
180.0	.18333	.00000	.01996
195.0	.18037	.00013	.01964
210.0	.15838	.00024	.01692
225.0	.08510	.00023	.00927
240.0	.05792	.00027	.00631
255.0	.07197	.00071	.00784
270.0	.00000	.00074	.00000
285.0	.03811	.00038	.00415
300.0	.25658	.00118	.02793
315.0	.59325	.00157	.06459
330.0	.84926	.00130	.09247
345.0	.96984	.00069	.10560
360.0	1.00000	.00000	.10888

E Z SURFACE(MEASURED)

PHI	EZ/EZM	DB.
.0	1.000	.00
11.2	.977	-.20
22.5	.944	-.50
33.7	.841	-1.50
45.0	.708	-3.00
56.3	.562	-5.01
67.5	.398	-8.00
78.7	.355	-9.00
90.0	.316	-10.01
101.2	.316	-10.01
112.5	.282	-11.00
123.7	.251	-12.01
135.0	.282	-11.00
146.2	.282	-11.00
157.5	.224	-13.00
168.7	.100	-20.00
180.0	.100	-20.00
191.2	.100	-20.00
202.5	.224	-13.00
213.8	.282	-11.00
225.0	.282	-11.00
236.3	.251	-12.01
247.5	.282	-11.00
258.7	.316	-10.01
270.0	.316	-10.01
281.2	.355	-9.00
292.5	.398	-8.00
303.7	.562	-5.01
315.0	.708	-3.00
326.2	.841	-1.50
337.5	.944	-.50
348.7	.977	-.20

TABLE 2.1 (CONTINUED)

FAR FIELD PATTERN OF BEVERAGE ANTENNA OVER FRESH WATER

D/LAMDAC = .0480 L1/LAMDAC = .960 RL = 280.08HMS

FREQUENCY = 144.1MHZ PE = .097 ALFAL/BETAL = .0348 BETAL/BETAO = 1.009

E THETA SPACE(THEORY)

THETA	ETH/ETHM
.0	.000
5.0	.329
10.0	.461
15.0	.540
20.0	.619
25.0	.674
30.0	.756
35.0	.842
40.0	.923
45.0	.982
50.0	1.000
55.0	.961
60.0	.851
65.0	.679
70.0	.451
75.0	.166
80.0	.146
85.0	.343
90.0	.502
95.0	.588
100.0	.592
105.0	.527
110.0	.415
115.0	.283
120.0	.156
125.0	.062
130.0	.069
135.0	.114
140.0	.135
145.0	.142
150.0	.138
155.0	.129
160.0	.119
165.0	.107
170.0	.091
175.0	.065
180.0	.000

E FIELDS SURFACE(THEORY)

PHI	EZ/EZM	EFI/EZM	ERO/EZM
.0	1.00000	.00000	.1C888
15.0	.97724	.00069	.1C640
30.0	.87392	.00134	.C9518
45.0	.69964	.00167	.C6886
60.0	.28233	.00130	.C3074
75.0	.02910	.00029	.CC317
90.0	.00000	.00069	.CC000
105.0	.07461	.00074	.CC812
120.0	.05149	.00024	.CC561
135.0	.07168	.00019	.CC780
150.0	.16027	.00025	.C1745
165.0	.19355	.00014	.C2107
180.0	.19862	.00000	.C2163
195.0	.19355	.00014	.C2107
210.0	.16027	.00025	.C1745
225.0	.07168	.00019	.CC780
240.0	.05149	.00024	.CC561
255.0	.07461	.00074	.CC812
270.0	.00000	.00069	.CC000
285.0	.02910	.00029	.CC317
300.0	.28233	.00130	.C3074
315.0	.62964	.00167	.C6886
330.0	.87392	.00134	.C9518
345.0	.97724	.00069	.1C640
360.0	1.00000	.00000	.1C888

E Z SURFACE(MEASURED)

PHI	EZ/EZM	DB.
.0	1.000	.00
10.0	1.000	.00
20.0	.944	-.50
30.0	.841	-1.50
40.0	.668	-3.50
50.0	.422	-7.49
60.0	.251	-12.01
70.0	.237	-12.51
80.0	.237	-12.51
90.0	.211	-13.51
100.0	.150	-16.48
110.0	.119	-18.49
120.0	.119	-18.49
130.0	.133	-17.52
140.0	.133	-17.52
150.0	.094	-20.54
160.0	.084	-21.51
170.0	.084	-21.51
180.0	.084	-21.51
190.0	.084	-21.51
200.0	.084	-21.51
210.0	.094	-20.54
220.0	.133	-17.52
230.0	.133	-17.52
240.0	.119	-18.49
250.0	.119	-18.49
260.0	.150	-16.48
270.0	.211	-13.51
280.0	.237	-12.51
290.0	.237	-12.51
300.0	.251	-12.01
310.0	.422	-7.49
320.0	.668	-3.50
330.0	.841	-1.50
340.0	.944	-.50
350.0	1.000	.00

FAR FIELD PATTERN OF BEVERAGE ANTENNA OVER FRESH WATER

D/LAMDAC = .0960 L1/LAMDAC = .960 RL = 307.08HMS

FREQUENCY = 144.1MHZ PE = .097 ALFAL/BETAL = .0162 BETAL/BETAO = 1.002

E THETA SPACE(THEORY)

THETA	ETH/ETHM
.0	.000
5.0	.191
10.0	.269
15.0	.327
20.0	.395
25.0	.448
30.0	.604
35.0	.732
40.0	.855
45.0	.952
50.0	1.000
55.0	.981
60.0	.883
65.0	.707
70.0	.487
75.0	.199
80.0	.107
85.0	.344
90.0	.521
95.0	.613
100.0	.617
105.0	.599
110.0	.523
115.0	.378
120.0	.137
125.0	.025
130.0	.069
135.0	.114
140.0	.138
145.0	.136
150.0	.122
155.0	.103
160.0	.086
165.0	.079
170.0	.059
175.0	.029
180.0	.000

E FIELDS SURFACE(THEORY)

PHI	EZ/EZM	EFI/EZM	ERO/EZM
.0	1.00000	.00000	.1C888
15.0	.97835	.00070	.1C682
30.0	.87748	.00134	.C9554
45.0	.63451	.00168	.C4909
60.0	.28510	.00131	.C3104
75.0	.02614	.00026	.CC285
90.0	.00000	.00068	.CC000
105.0	.07408	.00073	.CC8C7
120.0	.04439	.00020	.CC483
135.0	.07867	.00021	.CC857
150.0	.17675	.00027	.C1924
165.0	.21453	.00015	.C2336
180.0	.22085	.00000	.C2405
195.0	.21453	.00015	.C2336
210.0	.17675	.00027	.C1924
225.0	.07867	.00021	.CC857
240.0	.04439	.00020	.CC483
255.0	.07408	.00073	.CC8C7
270.0	.00000	.00068	.CC000
285.0	.02614	.00026	.CC285
300.0	.28510	.00131	.C3104
315.0	.63451	.00168	.C4909
330.0	.87748	.00134	.C9554
345.0	.97835	.00070	.1C682
360.0	1.00000	.00000	.1C888

E Z SURFACE(MEASURED)

PHI	EZ/EZM	DB.
.0	1.000	.00
8.2	1.000	.00
16.4	.966	-.30
24.7	.944	-.50
32.9	.813	-1.80
41.1	.631	-4.00
49.3	.398	-8.00
57.5	.282	-11.00
65.8	.224	-13.00
74.0	.224	-13.00
82.2	.224	-13.00
90.4	.178	-14.99
98.6	.141	-17.02
106.9	.126	-17.99
115.1	.141	-17.02
123.3	.158	-16.03
131.5	.126	-17.99
139.7	.089	-21.01
148.0	.089	-21.01
156.2	.112	-19.02
164.4	.126	-17.99
172.6	.141	-17.02
180.8	.141	-17.02
189.1	.141	-17.02
197.3	.126	-17.99
205.5	.112	-19.02
213.7	.089	-21.01
221.9	.089	-21.01
230.2	.126	-17.99
238.4	.158	-16.03
246.6	.141	-17.02
254.8	.126	-17.99
263.0	.141	-17.02
271.2	.178	-14.99
279.5	.224	-13.00
287.7	.224	-13.00
295.9	.224	-13.00
304.1	.282	-11.00
312.4	.398	-8.00
320.6	.631	-4.00
328.8	.813	-1.80
337.0	.944	-.50
345.2	.966	-.30
353.5	1.000	.00

TABLE 2.1 (CONTINUED)

FAR FIELD PATTERN OF BEVERAGE ANTENNA OVER FRESH WATER

C/LAMDAC = .2AC1 L1/LAMDAC = .96C RL = 372.08MMS

FREQUENCY = 144.1MHZ PE = .097 ALFAL/BETAL = .C086 BETAL/BETAO = 1.C01

E THETA SPACE(THEORY)

THETA	ETH/ETHM
.0	.C0
5.0	.197
10.0	.143
15.0	.209
20.0	.302
25.0	.434
30.0	.584
35.0	.739
40.0	.872
45.0	.964
50.0	1.000
55.0	.963
60.0	.849
65.0	.667
70.0	.437
75.0	.175
80.0	.C8C
85.0	.297
90.0	.455
95.0	.541
100.0	.551
105.0	.496
110.0	.394
115.0	.266
120.0	.133
125.0	.028
130.0	.057
135.0	.109
140.0	.121
145.0	.129
150.0	.112
155.0	.087
160.0	.062
165.0	.042
170.0	.C2C
175.0	.C27
180.0	.C3C

E FIELD SURFACE(THEORY)

PHI	EZ/EZM	EFI/EZM	ERB/EZM
.0	1.00000	.CCCCC	.1C888
15.0	.97908	.C007C	.1C660
30.0	.87992	.CC135	.C9881
45.0	.63807	.CC169	.C6947
60.0	.28758	.CC132	.C3131
75.0	.C2592	.CC026	.CC282
90.0	.00000	.CCC68	.CCCCC
105.0	.07513	.CCC74	.CC818
120.0	.C4689	.CCC22	.CC811
135.0	.07344	.CCC19	.CC8CC
150.0	.14879	.CC026	.C1838
165.0	.20438	.CCC15	.C2225
180.0	.20987	.CCCCC	.C2285
195.0	.20438	.CCC15	.C2225
210.0	.16879	.CC026	.C1838
225.0	.C7344	.CCC19	.CC8CC
240.0	.C4689	.CCC22	.CC811
255.0	.C7513	.CCC74	.CC818
270.0	.00000	.CCC68	.CCCCC
285.0	.02592	.CCC26	.CCF82
300.0	.28758	.CC132	.C3131
315.0	.63807	.CC169	.C6947
330.0	.87992	.CC135	.C9881
345.0	.97908	.CC07C	.1C660
360.0	1.00000	.CCCCC	.1C888

E Z SURFACE(MEASURED)

PHI	EZ/EZM	DB.
.0	.944	-.5D
10.0	.944	-.5D
20.0	1.000	.00
30.0	.944	-.5D
40.0	.841	-1.5D
50.0	.668	-3.5D
60.0	.376	-8.5D
70.0	.188	-14.5Z
80.0	.133	-17.5Z
90.0	.133	-17.5Z
100.0	.168	-15.4Y
110.0	.168	-15.4Y
120.0	.150	-16.4X
130.0	.1C6	-19.4Y
140.0	.119	-18.4Y
150.0	.168	-15.4Y
160.0	.168	-15.4Y
170.0	.211	-13.8I
180.0	.211	-13.8I
190.0	.211	-13.8I
200.0	.168	-15.4Y
210.0	.168	-15.4Y
220.0	.119	-18.4Y
230.0	.1C6	-19.4Y
240.0	.150	-16.4X
250.0	.168	-15.4Y
260.0	.168	-15.4Y
270.0	.133	-17.5Z
280.0	.133	-17.5Z
290.0	.188	-14.5Z
300.0	.376	-8.5D
310.0	.668	-3.5D
320.0	.841	-1.5D
330.0	.944	-.5D
340.0	1.000	.00
350.0	.944	-.5D

FAR FIELD PATTERN OF BEVERAGE ANTENNA OVER DRY EARTH

C/LAMDAC = .C096 L1/LAMDAC = .96C RL = 216.08MMS

FREQUENCY = 144.1MHZ PE = .C38

E Z SURFACE(MEASURED)

PHI	EZ/EZM	DB.
.0	1.CCC	.CC
15.0	.977	-.2D
30.0	.904	-.8D
45.0	.7C8	-3.CC
60.0	.466	-11.5C
75.0	.191	-17.CE
90.0	.1CC	-2C.CC
105.0	.C86	-21.C4
120.0	.C63	-24.C1
135.0	.C67	-23.4B
150.0	.C79	-22.CB
165.0	.1C6	-19.4Y
180.0	.1C6	-19.4Y
195.0	.119	-18.4Y
210.0	.1C6	-19.4Y
225.0	.C8C	-21.8I
240.0	.C75	-22.8C
255.0	.C38	-28.4G
270.0	.133	-17.5Z
285.0	.168	-15.4Y
300.0	.376	-8.5D
315.0	.75C	-2.5D
330.0	.944	-.5D
345.0	.977	-.2D

FAR FIELD PATTERN OF BEVERAGE ANTENNA OVER DRY EARTH

C/LAMDAC = .C192 L1/LAMDAC = .96C RL = 240.08MMS

FREQUENCY = 144.1MHZ PE = .C38

E Z SURFACE(MEASURED)

PHI	EZ/EZM	DB.
.0	1.CCC	.CC
15.0	.918	-.7D
30.0	.841	-1.5D
45.0	.501	-6.CC
60.0	.237	-12.8I
75.0	.C94	-2C.6A
90.0	.038	-28.4D
105.0	.045	-26.9A
120.0	.C68	-23.3A
135.0	.071	-22.9Y
150.0	.118	-18.4P
165.0	.126	-17.9B
180.0	.126	-17.9B
195.0	.126	-17.9B
210.0	.119	-18.4P
225.0	.071	-22.9Y
240.0	.C68	-23.3A
255.0	.C68	-23.9A
270.0	.C38	-28.4D
285.0	.C94	-2C.6A
300.0	.237	-12.8I
315.0	.5C1	-6.CC
330.0	.841	-1.5D
345.0	.918	-.7D

TABLE 2.1 (CONTINUED)

FAR FIELD PATTERN OF BEVERAGE ANTENNA OVER DRY EARTH

D/LAMDAC = .04PC L1/LAMDAC = .96C RL = 270.08MHS

FREQUENCY = 144.1MHZ PE = .C38

E Z SURFACE(MEASURED)

PHI	EZ/EZM	DB.
.0	1.CCC	.CC
15.C	1.CCC	.CC
30.0	.P61	-1.3C
45.0	.525	-5.6C
60.0	.216	-13.31
75.C	.C78	-22.85
90.C	.C51	-25.85
105.C	.C78	-22.85
12C.0	.C78	-22.85
135.0	.C77	-22.27
150.0	.C81	-21.83
165.C	.1CC	-2C.CC
180.C	.1CC	-2C.CC
195.0	.1CC	-2C.CC
210.0	.C81	-21.83
225.0	.C77	-22.27
24C.0	.C78	-22.85
255.0	.C78	-22.85
270.C	.C51	-25.85
285.C	.C78	-22.85
300.0	.216	-13.31
315.0	.525	-5.6C
33C.0	.861	-1.3C
345.C	1.CCC	.CC

FAR FIELD PATTERN OF BEVERAGE ANTENNA OVER DRY EARTH

D/LAMDAC = .C96C L1/LAMDAC = .56C RL = 335.08MHS

FREQUENCY = 144.1MHZ PE = .C38

E Z SURFACE(MEASURED)

PHI	EZ/EZM	DB.
.0	1.CCC	.CC
15.C	.977	-.2C
30.C	.891	-1.CC
45.0	.7C8	-3.CC
6C.C	.31e	-1C.C1
75.C	.C33	-29.63
9C.C	.C56	-25.C4
105.C	.112	-19.C2
12C.0	.1C6	-19.49
135.0	.C5C	-26.C2
150.0	.C33	-29.63
165.C	.C79	-22.C5
180.C	.112	-19.C2
195.0	.C84	-21.51
210.0	.C33	-29.63
225.0	.C5C	-26.C2
24C.0	.1C6	-19.49
255.0	.112	-19.C2
27C.C	.C5e	-25.C4
285.0	.C33	-29.63
30C.0	.31e	-1C.C1
315.0	.7C8	-3.CC
33C.0	.891	-1.CC
345.C	.977	-.2C

FAR FIELD PATTERN OF BEVERAGE ANTENNA OVER DRY EARTH

D/LAMDAC = .24C1 L1/LAMDAC = .96C RL = 365.08MHS

FREQUENCY = 144.1MHZ PE = .C38

E Z SURFACE(MEASURED)

PHI	EZ/EZM	DB.
.0	.P13	-1.8C
15.C	1.CCC	.CC
3C.C	.P41	-1.5C
45.0	.724	-2.81
6C.C	.4C7	-7.81
75.0	.182	-14.PC
9C.C	.P8P	-1C.P1
105.C	.115	-18.75
12C.0	.1CP	-15.33
135.C	.129	-17.79
15C.0	.2C4	-13.81
165.0	.243	-12.29
18C.C	.P8P	-1C.81
195.0	.243	-12.29
21C.C	.2C4	-13.81
225.0	.129	-17.79
24C.C	.1CP	-15.33
255.C	.115	-18.79
27C.0	.28P	-1C.81
285.C	.182	-14.PC
3CC.C	.4C7	-7.81
315.C	.724	-2.81
33C.0	.P41	-1.8C
345.C	1.CCC	.CC

REFERENCES

[1] R. W. P. King, Fundamental Electromagnetic Theory. New York: Dover Press, 1965.

[2] R. M. Sorbello, "The Beverage wave antenna: currents, charges and admittances. Vol. I. Theoretical analysis; experimental equipment and system calibration. Vol. II. Experimental measurements," Rome Air Development Center Contract F19628-76-C-0057, Scientific Report No. 1, Division of Engineering and Applied Physics, Harvard University, Cambridge, Mass., February 1977.

[3] A. Sommerfeld, Partial Differential Equations in Physics. New York: Academic Press, 1949.

[4] A. Sommerfeld, "The propagation of waves in wireless telegraphy," Ann. der Phys., vol. 28, pp. 665-736, 1909.

[5] A. Sommerfeld, "The propagation of waves in wireless telegraphy," Jahrb. d. Drahtl. Tel., vol. 4, pp. 157-176, 1910.

[6] R. Bruno, "Graphs to Sommerfeld's attenuation formula for radio waves," Proc. I.R.E., vol. 18, pp. 391-402, 1930.

[7] A. Sommerfeld, "The propagation of waves in wireless telegraphy," Ann. der Phys., vol. 81, pp. 1135-1153, 1926.

[8] H. Weyl, "The propagation of electromagnetic waves over a plane conductor," Ann. der Phys., vol. 60, pp. 481-500, 1919.

[9] B. van der Pol, et al., "The propagation of electromagnetic waves over a plane earth," Ann. der Phys., vol. 6, pp. 273-294, 1930.

[10] K. A. Norton, "The propagation of radio waves over a plane earth," Nature, vol. 125, pp. 954-955, 1935.

[11] W. H. Wise, "The physical reality of Zenneck's surface waves," Bell Syst. Tech. Journal, vol. 16, pp. 35-44, 1937.

[12] C. R. Burrows, "Surface waves in radio propagation over a plane earth," Proc. I.R.E., vol. 25, pp. 219-229, 1937.

[13] K. A. Norton, "The propagation of radio waves over the surface of the earth and in the upper atmosphere, Part II," Proc. I.R.E., vol. 25, pp. 1203-1238, 1937.

[14] R. W. P. King, Theory of Linear Antennas. Cambridge, Mass.: Harvard University Press, 1955.

[15] W. H. Wise, "Asymptotic dipole radiation formulas," Bell Syst. Tech. Journal, vol. 8, pp. 662-671, 1929.

[16] M. T. Ma, Theory and Application of Antenna Arrays. New York: Wiley Interscience, 1974.

[17] Ramo, Whinnery and Van Duzer, Field and Waves in Communication Electronics. New York: Wiley Pub., 1965.

[18] M. Abramowitz and I. A. Stegun, Handbook of Mathematical Functions. New York: Dover Press, 1965.

[19] E. E. Altshuler, "The traveling-wave linear antenna," Ph.D. Thesis, Harvard University, Cambridge, Mass., 1961.

[20] G. Sinclair, "The transmission and reception of elliptically polarized waves," Proc. I.R.E., vol. 38, pp. 148-151, Feb. 1950.

[21] A. Baños, Jr., Dipole Radiation in the Presence of a Conducting Half-Space. New York: Pergamon Press, 1966.

[22] R. W. P. King, L. C. Shen and T. T. Wu, "The horizontal wire antenna over a conducting or dielectric half-space," Radio Science, vol. 9, pp. 701-709, 1974.

[23] T. K. Sarkar and B. J. Strait, "Analysis of arbitrarily oriented thin-wire antenna arrays over imperfect ground planes," AFCRL, Scientific Report No. 9, 1975.

[24] R. J. Lytle and D. L. Lager, "Numerical evaluation of Sommerfeld integrals," Lawrence Livermore Technical Report, October 1974.

[25] R. F. Hahn and J. G. Fikioris, "Impedance and radiation patterns of antennas above flat discs," IEEE Trans. Antennas Propagat., vol. AP-21, pp. 97-100, Jan. 1973.

MISSION
of
Rome Air Development Center

RADC plans and conducts research, exploratory and advanced development programs in command, control, and communications (C^3) activities, and in the C^3 areas of information sciences and intelligence. The principal technical mission areas are communications, electromagnetic guidance and control, surveillance of ground and aerospace objects, intelligence data collection and handling, information system technology, ionospheric propagation, solid state sciences, microwave physics and electronic reliability, maintainability and compatibility.

Printed by
United States Air Force
Hanscom AFB, Mass. 01731